COLLECTORS OF Pt, Pd AND Rh IN A S-POOR Fe–Ni–Cu SULFIDE SYSTEM AT 760°C: EXPERIMENTAL DATA AND APPLICATION TO ORE DEPOSITS

Anna PEREGOEDOVA[§]

*Institute of Mineralogy and Petrography, Siberian Branch of Russian Academy of Science,
Prospect Acad. Koptyug, 3, Novosibirsk, 630090, Russia, and Department of Earth Sciences,
Carleton University, 1125, Colonel By Drive, Ottawa, Ontario K1S 5B6, Canada*

Maryse OHNENSTETTER[¶]

*Centre National de la Recherche Scientifique, Centre de Recherches Pétrographiques et Géochimiques,
15, rue Notre Dame des Pauvres, BP20, F–54501 Vandoeuvre-lès-Nancy Cedex, France*

ABSTRACT

The phase relations within the Fe_9S_8–Ni_9S_8–Cu_9S_8 section of the system Fe–Ni–Cu–S at 760°C were investigated in silica glass tubes. A complete "quaternary" solid-solution (Hz–Iss) between heazlewoodite solid-solution $(Ni,Fe)_{3\pm x}S_2$ and intermediate $Cu_{1\pm x}Fe_{1\pm y}S_2$ solid-solution was established. The possibility of direct crystallization of pentlandite (Pn) from Cu-containing sulfide melt is unlikely, as no primary Pn was found to be stable in the high-temperature associations. Experiments performed at the same conditions with Pt, Pd or Rh added in small quantities reveal the contrasting behavior of platinum-group elements (PGE). Pt preferentially forms its own minerals, either Pt–Fe alloys in association with Fe-rich base-metal sulfides (BMS) or platinum sulfides in Ni- and Cu-rich assemblages. At 760°C, sulfur fugacity $[f(S_2)]$ varies from –10.5 $[\log f(S_2)]$ where γ(Fe,Ni,Pt) alloy is stable to $\log f(S_2) \geq$ –1.1 where $Cu(Pt,Ni)_2S_4$ is present. Palladium enters sulfide solid-solutions, with up to 1.5 at.% in Hz–Iss and 0.9–1.1 at.% in Ni-rich monosulfide solid-solution (Mss). The behavior of Rh is remarkable; it may concentrate in BMS, especially Mss, accounting for up to 2.6 at.% Rh, or form Rh alloys or sulfides, under very low or very high $f(S_2)$, respectively. The application of the present experiments to PGE-bearing sulfide deposits indicates that sulfide solid-solutions were in most cases the temporary collectors of the light PGE before the appearance of Pn. During subsolidus recrystallization of the high-temperature BMS, Pd and Rh partition into Pn or form their own secondary minerals. PGE deposits with a predominance of Pt–Fe alloys, such as those occurring in mantle rocks exposed in ophiolites (Corsica, New Caledonia) or kimberlites, and in layered complexes (*e.g.*, the Merensky Reef, Bushveld Complex) are consistent with derivation from a S-poor sulfide melt, yielding early-formed Pt–Fe alloys. A similar origin may be inferred for the alloy type of Pt mineralization, which occurs in some crustal sequences of ophiolites and in Alaskan-type complexes, despite the very low amount of BMS present. Even in these low-S deposits, high $f(S_2)$ may be reached locally as a result of the appearance of a Cu-rich sulfide liquid, derived by fractionation or by immiscibility from an original Fe-rich sulfide melt.

Keywords: system Fe–Ni–Cu–S, experiments, phase relations, sulfide solid-solutions, partitioning of Pt, Pd and Rh, sulfur fugacity, Pt–Fe alloys, platinum-group elements, mineralization.

SOMMAIRE

Les relations de phase dans la section Fe_9S_8–Ni_9S_8–Cu_9S_8 du système Fe–Ni–Cu–S ont été étudiées expérimentalement par la méthode des tubes de verre en silice, à la température de 760°C. Une solution solide complète "quaternaire" à quatre composants, entre la solution solide de heazlewoodite $(Ni,Fe)_{3\pm x}S_2$ et la solution solide intermédiaire $Cu_{1\pm x}Fe_{1\pm y}S_2$, a été mise en évidence. La cristallisation directe de pentlandite (Pn) à partir d'un liquide sulfuré contenant du cuivre est peu probable, la Pn primaire n'étant pas stable dans les conditions de hautes températures. Des expériences réalisées dans les mêmes conditions, avec Pt, Pd ou Rh ajoutés en petites quantités, ont permis de révéler le comportement contrasté de ces éléments. Le platine forme préférentiellement ses propres minéraux, soit des alliages de Pt–Fe en association avec des sulfures de métaux de base riches en Fe, soit des sulfures de Pt avec des sulfures de métaux de base plus riches en Ni et Cu. La fugacité en soufre à 760°C varie, de –10.5 [en $\log f(S_2)$] lorsque les alliages de Ni, Fe et Pt sont présents à des fugacités supérieures, à –1.1 lorsque des phases de type $Cu(Pt,Ni)_2S_4$ sont stables. Le palladium entre dans les solutions solides sulfurées, jusqu'à 1.5 at.% dans la Hz–Iss et 0.9–1.1 at.% dans la solution

---

[§] *Present address*: Department of Earth and Planetary Sciences, McGill University, Montreal, Quebec H3A 2A7, Canada. *E-mail address*: aperegoe@eps.mcgill.ca

[¶] *E-mail address*: mohnen@crpg.cnrs-nancy.fr

solide monosulfurée (Mss) riche en Ni. Le comportement du Rh est remarquable pour sa possibilité d'entrer dans les solutions solides sulfurées, surtout dans la Mss (jusqu'à 2.6 at.% de Rh), ou de former des alliages ou sulfures, respectivement sous des conditions de très faibles ou très fortes fugacités en soufre. L'application de ces travaux expérimentaux aux gisements sulfurés porteurs d'éléments du groupe du platine (EGP) indique que les solutions solides de sulfures sont dans la plupart des cas les collecteurs temporaires des EGP légers avant l'apparition de la Pn. Pendant la recristallisation des solutions solides sulfurées de hautes températures, Pd et Rh entrent dans la pentlandite ou forment leurs propres minéraux. Les gisements ou indices de Pt avec une prédominance d'alliages, comme ceux qui existent dans le manteau des ophiolites (Corse, Nouvelle-Calédonie) ou dans les kimberlites, et dans les intrusions rubanées, comme dans le Merensky Reef du complexe du Bushveld, dériveraient d'un magma sulfuré pauvre en soufre, qui donnerait des alliages formés à un stade précoce. Une origine semblable peut être retenue pour les types de minéralisation en EGP porteuses d'alliages de Pt, qui existent dans certaines séquences crustales des ophiolites et dans les complexes alaskéens, en dépit de la faible quantité de sulfures de métaux de base présente. Même dans ces gisements pauvres en soufre, des fugacités de soufre élevées peuvent être atteintes localement lors de la formation d'un liquide sulfuré riche en Cu, qui dériverait d'un liquide sulfuré originel riche en fer par fractionnement ou par immiscibilité.

Mots-clés: système Fe–Ni–Cu–S, expériences, relations de phases, solutions solides sulfurées, répartition de Pt, Pd et Rh, fugacité en soufre, alliages de Pt et Fe, minéralisation en éléments du groupe du platine.

INTRODUCTION

The system Fe–Ni–Cu–S is of utmost importance to understand the origin of sulfide ores and related PGE mineralization. Numerous experimental studies of this system have been undertaken over the temperature interval of 1100°–840°C to investigate the behavior of platinum-group elements in the presence of a sulfide liquid (Fleet & Stone 1991, Fleet *et al.* 1993, Li *et al.* 1996, Barnes *et al.* 1997, Ebel & Campbell 1998, Peregoedova 1998). These studies provide important insights into the early stage of fractional crystallization processes, which are supposedly responsible for the metal zonation observed in PGE-bearing sulfide deposits. Little is known about more advanced stages of fractionation, where a small amount of residual sulfide liquid is still present. At the temperature of interest in the present study (760°C), the presence of a sulfide liquid has been questioned as well as the behavior of PGE, and the phase relations between the stable sulfide solid-solutions within the Fe–Ni–Cu–S tetrahedron. The mode of formation of pentlandite and its upper stability-limit were particularly controversial (Karup-Møller & Makovicky 1995, Naldrett *et al.* 1997). Whether pentlandite crystallized from a Cu-bearing sulfide melt at high temperatures (Distler *et al.* 1977), with the maximum stability-limit located at 865°±3°C (Sugaki & Kitakaze 1998), or whether it was produced by subsolidus reactions only, at temperatures below approximately 610°C (Kullerud 1963, Shewman & Clark 1970, Fyodorova & Sinyakova 1993), remains unclear.

The relationships between the high-temperature solid-solutions and pentlandite are important because a significant amount of Pd is incorporated in pentlandite in numerous Pt and Pd deposits. Mineral assemblages in Cu–Ni deposits generally represent the final product of various reactions that accompany successive steps of subsolidus re-equilibration, including the formation of pyrrhotite, pentlandite and various minerals of the chalcopyrite group.

In this paper, we experimentally investigate the distribution of Pt, Pd and Rh among base-metal sulfides over the temperature interval at which sulfide liquid is supposed to have just disappeared and when pentlandite might possibly exist. This study leads to the recognition of a high-temperature solid-solution, named Hz–Iss, with its composition lying between that of heazlewoodite solid-solution (Hz_{ss}) and intermediate solid-solution (Iss). The Hz–Iss phase generally appears by reaction between early *Mss* (monosulfide solid-solution) and liquid. The contrasting behavior of the PGE is underlined, notably the preference for Pt to form its own phase, either alloys or sulfides. The experimental results are applied to ore deposits, notably to those in which Pt–Fe alloys are the dominant phases. In addition, we tentatively discuss the origin of Pt–Fe–Ni–Cu alloys, which predominate in some ophiolites and Alaskan-type deposits, the source for most of the world's PGM-bearing placers.

We present this work in honor of Dr. Louis J. Cabri, in recognition of his numerous studies of platinum-group minerals, especially alloys, which are currently found in deposits and placers, and of the extent of solid solutions within Pt–Fe–Cu–Ni alloys. He was also involved in experimental studies dealing with phase relations in the system Cu–Fe–S, which is of critical importance for our understanding of PGE deposits. This paper complements the invaluable work done by Louis to determine conditions of formation of PGE alloys and sulfides formed in a S-undersaturated section of the system Fe–Ni–Cu–S.

BACKGROUND INFORMATION

Most of our knowledge of the system Fe–Ni–Cu–S is based on extrapolation from the three ternary subsystems Fe–Ni–S, Cu–Fe–S, and Cu–Ni–S. At temperatures relevant to the crystallization of magmatic sulfides, monosulfide [$(Fe,Ni)_{1\pm x}S$] (Mss) and heazlewoodite [$(Ni,Fe)_{3\pm x}S_2$] (Hz_{ss}) solid-solutions are the two main

solid phases in the system Fe–Ni–S (Naldrett & Kullerud 1967, Naldrett *et al.* 1967, Hsieh *et al.* 1982, Fyodorova & Sinyakova 1993, Karup-Møller & Makovicky 1995, 1998). The system Cu–Fe–S is dominated by intermediate $[Cu_{1\pm x}Fe_{1\pm y}S_2]$ (Iss), bornite $[Cu_{5\pm x}Fe_{1\pm y}S_4]$ (Bn_{ss}) and pyrrhotite $[Fe_{1-x}S]$ (Po_{ss}) solid-solutions (Kullerud *et al.* 1969, Cabri 1973, Barton 1973). All of these phases display an appreciable extent of solid solution in the quaternary system Fe–Ni–Cu–S (Craig & Kullerud 1969, Hill 1983, Fleet & Pan 1994, Ebel & Naldrett 1997). Fleet & Pan (1994) reported the existence of a ternary (Fe,Cu,Ni)S solid-solution intermediate between Iss and Mss at and below 850°C; its stoichiometry is close to that of cubanite ($CuFe_2S_3$). During crystallization, monosulfide solid-solution is the first phase to appear at high temperatures from an Fe-rich sulfide liquid, before Hz_{ss} or Iss form by reaction between Mss and the residual liquid in the systems Fe–Ni–S and Cu–Fe–S, respectively (Kullerud *et al.* 1969, Fyodorova & Sinyakova 1993, Ebel & Naldrett 1996, 1997).

A contrasting behavior of platinum-group elements (PGE) is reported during crystallization of Mss from a sulfide melt containing PGE at "wt.%" levels. Experiments in the system Fe–Ni–S and, more recently, in the system Fe–Ni–Cu–S have shown that the partition coefficients for PGE between Mss and sulfide liquid strongly depend on $f(S_2)$ and are moderately temperature-dependent (Barnes *et al.* 1997, Peregoedova 1998). Li *et al.* (1996) showed that the partition coefficients of Ir, Rh, Pt and Pd between monosulfide solid-solution and sulfide liquid increase with increasing bulk sulfur content in the system at 1000° and 1100°C (S in the experiments varying from 47 to 58 at.%). In addition, they emphasized the compatible behavior of Ir and Rh, and the incompatible behavior of Pt, Pd and Cu under S-saturated conditions. These conclusions agree with the results of Fleet *et al.* (1993), who performed experiments in the system Fe–Ni–Cu–S with PGE at concentration levels more typical of natural samples (17–53 ppm of each PGE). They showed that under high $f(S_2)$, both Pt and Pd are partitioned into a sulfide liquid, whereas the remaining PGE enter into Mss. A contrasting pattern of behavior of Pt and Pd is found under low $f(S_2)$; Pt forms Pt–Fe alloys, whereas Pd and Rh are concentrated in the sulfide liquid (Fleet & Stone 1991, Fleet *et al.* 1993).

In the present study, we investigated the metal-rich Fe_9S_8–Ni_9S_8–Cu_9S_8 (Me_9S_8) section of the system Fe–Ni–Cu–S, corresponding to the metal:S ratio of pentlandite, at 760°C (Fig. 1). Experiments cover a large compositional field in which base-metal contents vary regularly from 11.8 to 41.2 at.% (Cu + Ni). This includes a domain of Cu-rich composition in which pentlandite is considered to appear as a magmatic phase. Two sets of experiments were done: the first, without PGE added, was designed to determine the stable sulfide assemblages at 760°C in the compositional field of interest;

the second, containing PGE, was performed to study how Pt and the light platinum-group elements (Pd and Rh) partition between these phases. The PGE were added in subordinate concentrations (0.5–1 wt.%), which is very far from natural "ppm" levels of PGE in natural ores, but allows the use of the electron microprobe technique for analysis of the run products (Distler *et al.* 1988, Kolonin *et al.* 1993, Fleet *et al.* 1993, Li *et al.* 1996, Sinyakova *et al.* 1996, Ebel & Campbell 1998, Peregoedova & Ohnenstetter 1999). This method allowed us to study the behavior of PGE in multicomponent systems, and does not affect the phase relations of the base-metal sulfides. According to Kolonin (1998), two subsystems can be defined when a PGE is added in minor amounts to a multicomponent system: one system comprises essential macrocomponents that are the base-metal sulfides, and the second system comprises PGE as trace microcomponents "forming quantitatively strongly subordinate independent mineral phases of platinum-group elements or dispersed in crystalline lattices of BMS as microimpurities". Ebel & Campbell (1998) studied high-temperature partitioning behavior of trace quantities (ppm) of rhodium and ruthenium with the use of the laser-ablation ICP–MS method in the system Fe–Ni–Cu–S. At temperatures between 1150° and 1100°C, partition coefficients for rhodium and ruthenium obtained in their study are consistent with previous investigations conducted at "wt.%" concentration levels of PGE. This finding indicates that the "wt.%"-level approach to partitioning of PGE can also be applied to trace concentration levels typical of natural PGE-bearing sulfide ores.

Experimental Methods

Thirty-three samples with compositions lying in the Me_9S_8 section of the system Fe–Ni–Cu–S were synthesized in evacuated silica glass tubes from pure elements: high-purity iron (99.99%), high-purity nickel shavings (99.99%), high-purity copper foil (99.99%), special-purity sulfur (99.9999%), after additional drying under vacuum. Vertical furnaces were used for the PGE-free and Pt-containing experiments, whereas Pd- and Rh-containing samples were annealed in horizontal furnaces. After preheating the mixture of base metals and sulfur at 300°C for three days and subsequent melting at 1100°C, the samples were slowly cooled to room temperature over a period of one day. About 0.3 g of the synthesized samples were resealed and annealed at 760°C for 14 days in order to determine the phase relations in the PGE-free sulfide system, whereas nearly 1 g of material was used for further experiments with the PGE. Platinum was added in quantity of 1 wt.% (0.23 at.%), followed by melting at 1100°C and slow cooling for three weeks. Approximately 0.3 g of these samples were then annealed at 760°C in evacuated silica glass tubes for 14 days. The inner diameter of silica glass tubes used for annealing at 760°C was 3 mm, with a
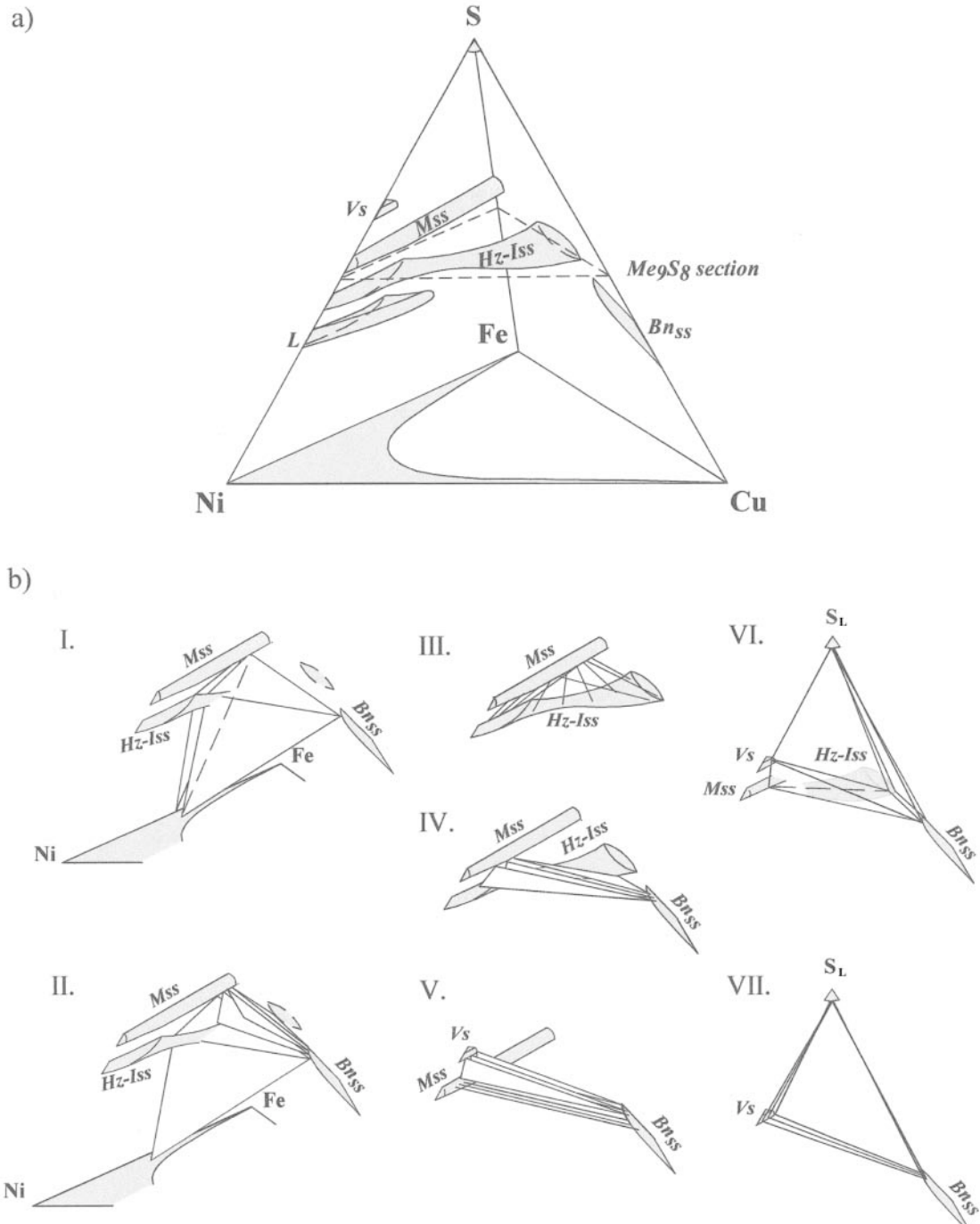
FIG. 1. (a) Phases stable in the central part of the system Fe–Ni–Cu–S at 760°C. (b) Stable associations in the Me_9S_8 section at 760°C. I. Fe-Mss + Hz–Iss + γ(Fe,Ni), Fe-Mss + Hz–Iss + γ(Fe,Ni) + Bn$_{ss}$. II. Fe-Mss + Hz–Iss + Bn$_{ss}$. III. Mss + Hz–Iss. IV. Ni-Mss + Hz–Iss + Bn$_{ss}$. V. Ni-Mss + Bn$_{ss}$, Ni-Mss + Bn$_{ss}$ + Vs. VI. Hz–Iss + Bn$_{ss}$ + S$_L$, Hz–Iss + Bn$_{ss}$ + S$_L$ + Vs, Hz–Iss + Bn$_{ss}$ + Vs + Ni-Mss. VII. Bn$_{ss}$ + Vs + S$_L$. The following abbreviations are used here and elsewhere in the paper: Mss: monosulfide solid-solution (ss); Po$_{ss}$: pyrrhotite ss, Hz$_{ss}$: heazlewoodite ss, Iss: intermediate ss, Hz–Iss: quaternary ss, Bn$_{ss}$: bornite ss, Po: pyrrhotite, Hz: heazlewoodite, Pn: pentlandite, Vs: vaesite, Cp: chalcopyrite, Bn: bornite, S$_L$: sulfur liquid, L: sulfide liquid.

wall thickness of 1 mm. After annealing, the tubes with the samples were quenched in a mixture of water and ice. Quenching to room temperature took about 3 seconds.

The same procedure was repeated to prepare samples containing 1 wt.% (0.44 at.%) of Pd or Rh. Therefore, all experiments were performed with three different metals added, and the base-metal sulfide assemblages were found to be reproducible. The resulting phase-assemblages were analyzed by electron microprobe. Profiles across the representative products were done to test for compositional homogeneity.

Equilibrium conditions

Lines of evidence indicative of the attainment of equilibrium in both sets of experiments are the following:

(1) The assemblages are reproducible in duplicate experiments of the same duration.

(2) On heating and cooling, reactions are reversible from one equilibrium assemblage to another. The temperatures of phase reactions in individual samples were determined by thermal analysis (DTA). Additional experiments were carried out at different temperatures, 900°C and 550°C, respectively, and the changes in phase assemblages occurring at these temperatures were noted.

(3) The composition of base-metal sulfides and coexisting platinum-group minerals is constant throughout the sample.

(4) The distribution of the PGE between base-metal sulfides varies according to the initial metal ratio of the experimental charge in a manner similar to that described in experiments conducted at higher temperatures (Fleet & Stone 1991, Peregoedova 1998).

(5) The duration of annealing (two weeks) is sufficient for achievement of equilibrium in the system Fe–Ni–Cu–S at the temperature of 760°C. In addition, two series of experiments were conducted at the same temperature (760°C) for 14 and 21 days, respectively, but in the part of the system Fe–Ni–Cu–S richer in sulfur (48.5 at.% S). No changes in phase relationships were detected after increasing the time of annealing.

Determination of sulfur fugacity

Sulfur fugacity was estimated using the equation of Toulmin & Barton (1964), which correlates the composition of pyrrhotite, fugacity of sulfur and temperature. Toulmin & Barton (1964) showed that this method makes it possible to determine sulfur fugacity for many reactions in the stability field of pyrrhotite. In the present study, all phase assemblages lie within the stability field of pyrrhotite, except in the part of the Me_9S_8 section richest in Cu, where pyrite replaces pyrrhotite as a stable phase. In this case, the equation of Toulmin & Barton (1964) could not be used.

During the experiments, the following procedure was employed. Pyrrhotite was synthesized separately and checked by microscopic examination and X-ray diffraction for its composition and homogeneity. Then, an open tube containing about 10–30 mg of pyrrhotite powder was placed in a larger tube filled with a sample along the Me_9S_8 section in such a manner that both the sample and the pyrrhotite coexisted with one common gas-phase but were not in physical contact with each other (tube-in-tube method). These "double tubes" were evacuated, sealed, annealed at 760°C for two weeks, and then quenched. In the course of annealing, the composition of pyrrhotite from the inner tube changed owing to the emission of sulfur vapor from the sample. The final composition of pyrrhotite was determined by X-ray diffraction by using its d_{102} value, and the actual log $f(S_2)$ was calculated. According to Toulmin & Barton (1964), the total error in the estimate of log $f(S_2)$ from the composition of pyrrhotite is about ±0.35.

The use of the composition of pyrrhotite to determine the sulfur fugacity was previously tested for the lead – lead sulfide equilbrium (Toulmin & Barton 1964), monosulfide solid-solution (Naldrett 1967) and for experimental sulfide assemblages in the Pt-bearing Fe–Ni–S system (Sinyakova *et al.* 1996). In the latter case, the fugacity of sulfur for phase associations containing distinct platinum-group minerals was determined by this method for experiments under dry conditions. The results reported are in good agreement with those obtained by Evstigneeva & Tarkian (1996) for Pt-phases synthesized under hydrothermal conditions. These results support the utilization of the composition of pyrrhotite to determine the fugacity of sulfur.

Sample identification

Microscopic examination, thermal analysis and X-ray diffraction were used to study the compositions of associated phases and the temperature of the reactions. The accuracy of temperature determination by thermal analysis was ±5°C. Both derivative and differential methods of thermal analysis were applied using a DTA device at the Institute of Mineralogy and Petrology in Novosibirsk, Russia (Alabuzhev 1969). Details of this DTA technique are given by Sinyakova *et al.* (1999). In the present study, PGE-free samples synthesized by melting with subsequent slow cooling to room temperature were used for thermal analysis. The temperatures of reactions and phase transitions have been determined during both heating the samples from room temperature to melting and upon their cooling with the furnace turned off. Only the temperatures of interest to this study are reported in this paper, including the temperatures of liquidus and the temperatures of formation of quaternary solid-solution Hz–Iss. For samples in the Ni-rich or Cu-rich areas of the Me_9S_8 section, these temperatures have been determined from cooling curves according to the method of Sinyakova *et al.* (1999).

X-ray diffraction was used for all PGE-free samples after melting followed by slow cooling, and for some of them after 760°C annealing and quenching to complement the identification of phases by microscopic examination and microprobe analysis. Electron-microprobe analyses were carried out using a Camebax SX50 instrument at the Institute of Mineralogy and Petrography, Novosibirsk, Russia and at the Service Commun de Microanalyse, Université de Nancy, France. The sulfides $CuFeS_2$ and FeS, FeNiCo alloy as well as Ni, Pt, Pd and Rh metals were used as standards. The analytical conditions were as follows: accelerating voltage 20 kV, beam current 20 nA for Fe, Ni, Cu, and S, and 100 nA for the PGE, counting times up to 60 s and spot diameter 3 μm. The data reduction was done using the PAP correction procedure (Pouchou & Pichoir 1984, 1991). A defocused electron beam (15–40 μm) was used to determine the bulk compositions of quenched sulfide solid-solutions. The detection limits of Pt, Pd and Rh were <0.1 wt.%. The standard deviations of the electron-microprobe analyses are presented in Table 1.

Partition coefficients of elements between coexisting monosulfide and quaternary solid-solutions were calculated using the following equation (e.g., for Pd): $D^{Mss/Hz-Iss}$ for Pd = wt.% of Pd in Mss / wt.% of Pd in Hz–Iss.

PHASE ASSEMBLAGES
IN THE TETRAHEDRON Fe–Ni–Cu–S AT 760°C

The starting composition, phase association and the average composition of phases coexisting in the Me_9S_8 section of the system Fe–Ni–Cu–S (i.e., PGE-free) at 760°C are reported in Table 2. Six phases are stable in the part of Me_9S_8 section studied: monosulfide $(Fe,Ni)_{1+x}S$, bornite $Cu_{5+x}Fe_{1+y}S_4$ and vaesite $(Ni,Fe)S_2$ solid-solutions, γ(Fe,Ni) alloy, sulfur liquid (S_L) and a quaternary $(Ni,Cu,Fe)_{3\pm x}S_2$ solid-solution that was identified during this study as a complete solid-solution between intermediate (Iss) and heazlewoodite (Hz_{ss}) solid-solutions (Fig. 1).

Quaternary solid-solution $(Ni,Cu,Fe)_{3\pm x}S_2$

The quaternary solid-solution (Hz–Iss) coexists with Mss in most parts of the section investigated (Fig. 1b, diagram III; Fig 2a) except for some Cu–Ni-rich or Fe-rich samples. Hz–Iss occurs in association with Mss and Bn_{ss} in Ni- and Cu-rich charges, with Bn_{ss} and S_L in the experiment richest in Cu, and with γ(Fe,Ni) alloy in experiments performed with the bulk composition richest in Fe (Figs. 1b, 2a). With decreasing bulk Ni-content of the samples, the Ni content of Hz–Iss in equilibrium with Mss decreases gradually from an Ni-rich (44.8 at.% Ni, 0 at.% Cu) to a Cu-rich (4.5 at.% Ni, 26.6 at.% Cu) composition (Fig. 3a). Where the bulk Cu-content exceeds 17.7 at.% and Bn_{ss} appears in association with Mss and Hz–Iss, the composition of Hz–Iss becomes very Cu-rich (33.1–36.7 at.%), close to that of S-poor intermediate solid-solution $[Cu_{1\pm x}Fe_{1+y}S_2]$, Iss. It is very likely that the quaternary solid-solution Hz–Iss includes the entire compositional range between Iss, previously described in the system Cu–Fe–S, and heazlewoodite solid-solution $[(Ni,Fe)_{3\pm x}S_2]$ (Hz_{ss}) known from the system Fe–Ni–S (Fig. 1a). In addition, there is a continuous variation in metal proportions from Hz_{ss} relevant to the system Fe–Ni–S, to Iss in the system Cu–Fe–S across the quaternary system Fe–Ni–Cu–S (Fig. 3, Table 2). No compositional gap can be identified in the range of S contents shown by Hz–Iss from Cu-poor to Cu-rich composition (Fig. 3b).

Hz–Iss appears to be an unquenchable phase like Iss and Hz_{ss}. According to the literature data on the systems Fe–Ni–S (Kullerud 1963, Fyodorova & Sinyakova 1993, Karup-Møller & Makovicky 1995) and Cu–Fe–S (Cabri 1973), Hz_{ss} and Iss undergo complex and rapid phase-transformations during quenching from high temperatures. The breakdown of Hz_{ss} results in the forma-

TABLE 1. STANDARD DEVIATIONS OF ELECTRON MICROPROBE ANALYSES
AT DIFFERENT ANALYZING CONDITIONS (IN AT.%).

Phases analyzed	Defocused electron beam (15-40 μm)							Narrow electron beam (2-3 μm)						
	Fe	Ni	Cu	Pt	Pd	Rh	S	Fe	Ni	Cu	Pt	Pd	Rh	S
Structures of decomposition of unquenchable BMS	0.3	0.3	0.3	0.02	0.05	0.02	0.3				-			
Quench products of BMS solid-solutions				-				0.5	0.6	0.3	-	0.08	0.04	0.2
Homogeneous PGE-bearing BMS				-				0.2	0.2	0.2	-	0.03	0.04	0.2
Platinum-group minerals				-				0.2	0.3	0.2	0.3	0.3	0.2	0.1

TABLE 2. THE RESULTS OF EXPERIMENTS CONDUCTED ALONG Me_9S_8 SECTION OF THE Fe-Ni-Cu-S SYSTEM.

N°	Starting composition, at.% Fe	Ni	Cu	T°C Hz-Iss form	T°C Melt.	log $f(S_2)$ at 760°C	BMS association at 760°C	Composition, at.% Fe	Ni	Cu	S
1	41.2	11.8	0	831	1066	-10.5	Mss	46.8	2.6	0	50.6
							Hzss*	25.1	29.8	0	45.1
2	35.3	17.7	0	830	1020	-7.5	γ(Fe,Ni)	no data			
							Mss	46.6	3	0	50.4
							Hzss*	27.9	25.1	0	47
3	29.4	23.5	0	862	999	-6.2	Mss	36.9	12.7	0	50.4
							Hzss*	20.6	34.6	0	44.8
4	23.5	29.4	0	864**	986	-5.7	Mss	34.3	15.4	0	50.3
							Hzss	19.2	36.4	0	44.4
5	17.7	35.3	0	844	938	-4.4	Mss	24.3	24.9	0	50.8
							Hzss	14.1	41.3	0	44.6
6	11.8	41.2	0	826	907	-4.1	Mss	15.9	33.9	0	50.2
							Hzss	9.8	44.8	0	45.4
7	41.2	5.9	5.9	no data		-10.5	Mss	47.2	1.5	0.9	50.4
							Hz-Iss*	27.3	17.9	11.9	42.9
							Bnss	no data			
8	35.3	11.8	5.9	no data		-7.5	γ(Fe,Ni)				
							Mss	43.1	5.4	1.6	49.9
							Hz-Iss	27.2	17.9	9.8	45.1
9	29.4	17.7	5.9			-5.7	Mss	37.6	10.6	1.6	50.2
							Hz-Iss	23.3	23.2	8.7	44.8
10	23.5	23.5	5.9	839	936	-4.6	Mss	30.7	17.5	1.6	50.2
							Hz-Iss	21.3	25.4	7.2	46.1
11	17.7	29.4	5.9	807	925	-4.1	Mss	22.5	26.1	0.7	50.7
							Hz-Iss	16.1	30.7	7.5	45.7
12	11.8	35.3	5.9	795	929	-3.7	Mss	14.5	33.9	0.8	50.8
							Hz-Iss*	9.9	42.7	1.6	45.8
							Bnss*	3.3	1.5	60.8	34.4
14	35.3	5.9	11.8	no data		-6.8	Mss	43.5	4.4	1.5	50.6
							Hz-Iss	24.6	7.4	23.9	44.1
15	29.4	11.8	11.8			-5.5	Mss	37.4	10.2	2.6	49.8
							Hz-Iss	25.8	11.9	17.4	44.9
16	23.5	17.7	11.8	835	929	-4.3	Mss	28.9	18.8	2.7	49.6
							Hz-Iss	21.7	17.1	16.2	45
17	17.7	23.5	11.8	873	907	-3.7	Mss	18.5	29.8	1.4	50.3
							Hz-Iss	16.6	28.9	8.5	46
							Bnss	11.3	1.7	47.1	39.9
18	11.8	29.4	11.8	807	898	-3.6	Mss	13.4	35.3	0.7	50.6
							Hz-Iss*	10.7	42.2	1.2	45.9
							Bnss*	3	1.5	61.6	33.9
19	35.3	0	17.7	no data		-5.7	Poss	46.3	0	3.1	50.6
							Iss*	31.2	0	20.6	48.2
							Bnss*	2.5	0	52.3	38.2
20	29.4	5.9	17.7	908	962	-4.6	Mss	38.6	8.2	3.1	50.1
							Hz-Iss	26.2	4.6	23.5	45.7
21	23.5	11.8	17.7	850	909	-3.7	Mss	29.4	18.3	2.2	50.1
							Hz-Iss	18.3	4.7	33.7	43.3
							Bnss	14.2	0.4	44.2	41.2
22	17.7	17.7	17.7	no data		-3.6	Mss	20.9	27.3	1.6	50.2
							Bnss	13.9	0.6	43.8	41.7
23	11.8	23.5	17.7	-	853	-3.1	Mss	12.1	35.5	0.8	51.6
							Bnss	10.9	4	43.9	41.2
24	29.4	0	23.5	877	937	-4.1	Iss	29.5	0	23.7	46.8
25	23.5	5.9	23.5	862		-2.8	Mss	26.5	18.5	4.6	50.4
							Hz-Iss	23	4.5	26.6	45.9
26	17.7	11.8	23.5	860		-1.7	Mss	20.9	25.2	2.6	51.3
							Hz-Iss	16.5	3.3	36.7	43.5
27	11.8	17.7	23.5	-	939	-1.1	Mss	12.5	31.8	3.6	52.1
							Bnss	12.5	2	43.4	42.1
28	23.5	0	29.4	-		-1.4	Iss	23.1	0	30.7	46.2
29	17.7	5.9	29.4	no data		>0	Mss***	15.9	25.2	10.3	48.6
							Hz-Iss	18.6	2.5	33.1	45.8
							Bnss	14.8	1.7	40	43.5
30	11.8	11.8	29.4	-	832	>0	Mss	12.8	32.9	2.5	51.8
							Bnss	12.4	0.2	46.3	41.1
31	17.7	0	35.3	no data		>0	Iss	18.7	0	36.2	45.1
							Bnss	15.3	0	41.5	43.2
32	11.8	5.9	35.3	-	873	>0	Vs	2	28.2	6.3	63.5
							Bnss	13.8	1.8	41.2	43.2
33	11.8	23.5	41.2	-	837	>0	Bnss	13.1	0	44.4	42.5
							S_L	-			

* The quench products of Hzss, Iss, Hz-Iss or Bnss were analyzed with the use of narrow electron beam (2-3 μm).

** The temperatures obtained by DTA upon cooling are shown in italic, the others temperatures have been determined during heating.

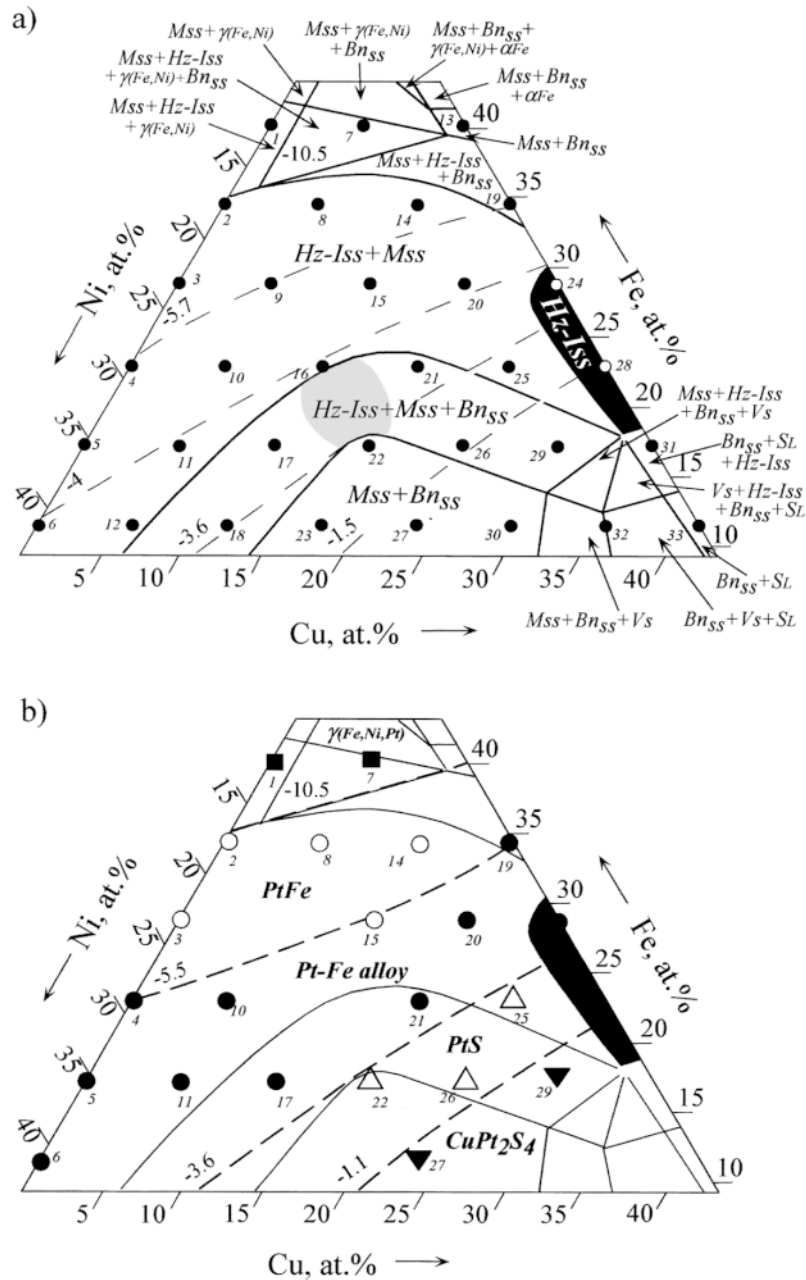*** The product of reaction between Mss and Hz-Iss was analyzed.

FIG. 2.   (a) Diagram schematically showing stability fields of phase assemblages in the Me_9S_8 section of the system Fe–Ni–Cu–S at 760°C. Dashed lines are used to schematically illustrate the isobars of sulfur fugacity in log $f(S_2)$ (atm). Dots indicate starting compositions and numbers of experimental runs. See explanation in the text for the grey region in the stability field of Hz–Iss + Mss + Bn_{ss}. (b) Platinum phases coexisting with base-metal sulfide solid-solutions stable in the Me_9S_8 section of the Pt-bearing system Fe–Ni–Cu–S at 760°C [solid squares: Pt-bearing γ(Fe,Ni) alloy, open circles: Pt–Fe alloys with composition close to PtFe, solid circles: Pt–Fe alloys with composition intermediate between PtFe and Pt_3Fe, open triangles: synthetic analogue of natural cooperite, PtS, and solid triangles: synthetic analogue of natural malanite, $CuPt_2S_4$. The dashed lines show schematically the boundary of stability domains of the platinum phases with corresponding limits of sulfur fugacity in log $f(S_2)$.

tion of pentlandite-bearing assemblages, and the break-down of Iss gives rise to various minerals of the chalcopyrite group. According to data for the system Cu–Fe–S (Cabri 1973), the phase Iss is quenchable only over a very limited area near the composition of cubanite, *i.e.,* where the starting bulk composition is richer in S than in the present study. In the present experiments, Hz–Iss was not preserved after quenching.
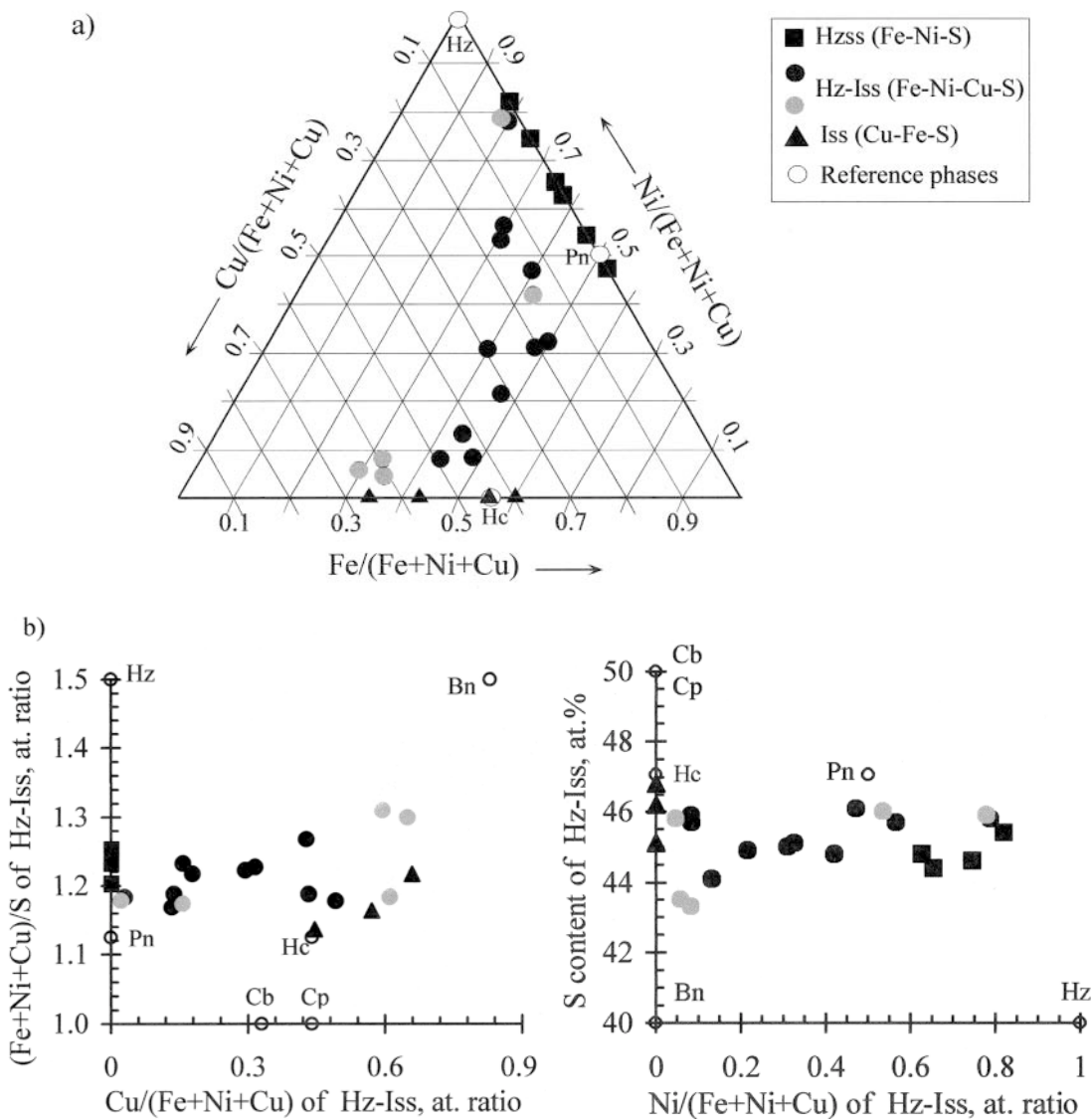

FIG. 3.   Continuous range of compositions transitional between heazlewoodite solid-solution (Hz$_{ss}$, in the system Fe–Ni–S) and intermediate solid-solution (Iss, in the system Cu–Fe–S) determined with an electron microprobe. (a) Projection of the Hz–Iss compositions at 760°C on the section with 45 at.% S of the system Fe–Ni–Cu–S. (b) The variations of metal:S ratio and total S contents of Hz–Iss, with different metal proportions [solid squares: the compositions of Hz$_{ss}$ in the assemblages stable along the Fe–Ni–S join of Me_9S_8 section; solid triangles: the compositions of Iss stable along the Cu–Fe–S join; solid circles: the compositions of Hz–Iss stable inside the Me_9S_8 section, together with Mss; grey circles: the compositions of Hz–Iss stable together with Mss and Bn$_{ss}$; open circles: reference compositions of pentlandite (Pn), heazlewoodite (Hz), cubanite (Cb), chalcopyrite (Cp), haycockite (Hc) and bornite (Bn)].

In polished sections, several exsolution-induced phases, which formed during the quench interval, can be seen within large single grains of the original solid-solution stable at 760°C. The assemblage of quench products depends on the initial composition of Hz–Iss before its breakdown, which is related to the bulk composition of the charges. For example, along the Fe_9S_8–Ni_9S_8 join, Hz_{ss} generally decomposes during quenching into pentlandite, heazlewoodite and γ(Fe,Ni) alloy (Fig. 4a). If Cu is added to the starting composition, lamellar or droplet-like grains of bornite and minerals of the chalcopyrite group appear together with Ni-bearing products of decomposition of Hz_{ss} and are interpreted as low-temperature exsolution products. This quench association further confirms that Hz_{ss} contains copper before quenching (Fig. 4b). With continuous increase of the bulk Cu content in the starting composition, the abundance of Cu-bearing phases increases among other quench products of Hz_{ss}. The gradual change of quench products of Hz_{ss} from those characteristic of the system Fe–Ni–S to those typical of Iss from the system Cu–Fe–S through the Me_9S_8 section is good evidence for the existence of a single quaternary solid-solution (Hz–Iss) at the temperature of interest in the present study. This inference is corroborated by the absence of two distinct quenched assemblages (textures) derived from distinct Hz_{ss} and Iss phases, in the central part of the section studied.

On the basis of literature data on the crystal structures of Hz_{ss} and Iss, mutual mixing to produce one continuous solid-solution is quite likely. Both high-temperature Iss and Hz_{ss} containing 20 at.% Fe have the face-centered cubic sphalerite-like structure (Kullerud 1963, Cabri 1973, Sinyakova $et\ al.$ 1991). At temperatures above 550°C, heazlewoodite ($Ni_{3\pm x}S_2$) has a crystal structure identical with that of high-temperature Iss (Liné & Huber 1963).

In the ternary systems Fe–Ni–S and Cu–Fe–S, both Hz_{ss} and Iss can crystallize as a result of a peritectic reaction between sulfide liquid and Mss or Po_{ss}, respectively (Kullerud $et\ al.$ 1969, Fyodorova & Sinyakova 1993). In the system Fe–Ni–S, Hz_{ss} forms in the temperature interval 876°–806°C (Fyodorova & Sinyakova 1993), whereas in the system Cu–Fe–S, Iss begins to form at 908°C (Dutrizac 1976). In the present study, a few experiments were conducted along the Me_9S_8 section at 900°, 870° and 840°C, and supplemented by thermal analyses to determine the upper stability-limit of Hz–Iss and its mode of formation. For Cu-poor samples, along the Fe_9S_8–Ni_9S_8 join (samples 1–6, Table 2), and those with Cu# ≤ 0.22 [Cu# = Cu/(Cu + Fe + Ni); samples 7–18, Table 2], the liquidus temperature decreases from 1066° to 896°C from Fe-rich to Ni-rich starting compositions. Quenching experiments at high temperatures (900°C for samples 1–12; 870°C for samples 17–18) indicate that Mss and sulfide liquid are
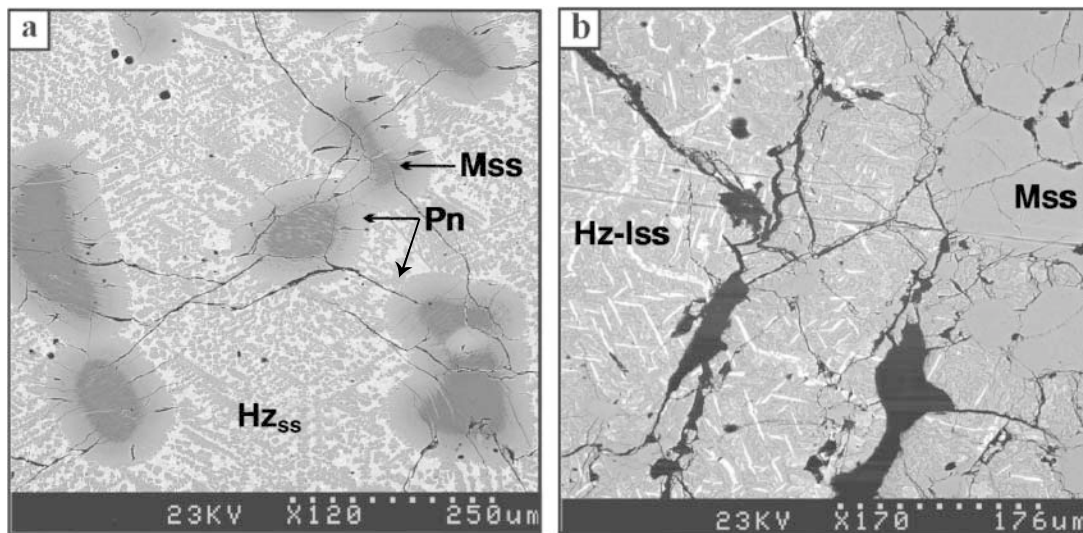

FIG. 4.   Back-scattered electron images. (a) Microstructure of quenched run-products with pentlandite (grey) and fine mixture of heazlewoodite with γ(Fe,Ni) alloy and probably godlevskite (light grey). Rounded grains of Mss host the fine lamellae of Pn. Note the reaction rims of Pn, located at contact between Mss and Hz_{ss} (sample 3 after quenching from 760°C). (b) Structure of breakdown products of Cu-containing quaternary solid-solution (Hz–Iss), with lamellae of bornite (white) oriented in three crystallographic directions. Other quenched products of Hz–Iss are the fine mixture with Pn (light grey) and different phases of the chalcopyrite group (dark grey). Large homogeneous grain in the right part of the image belongs to monosulfide solid-solution (sample 10, after quenching from 760°C).
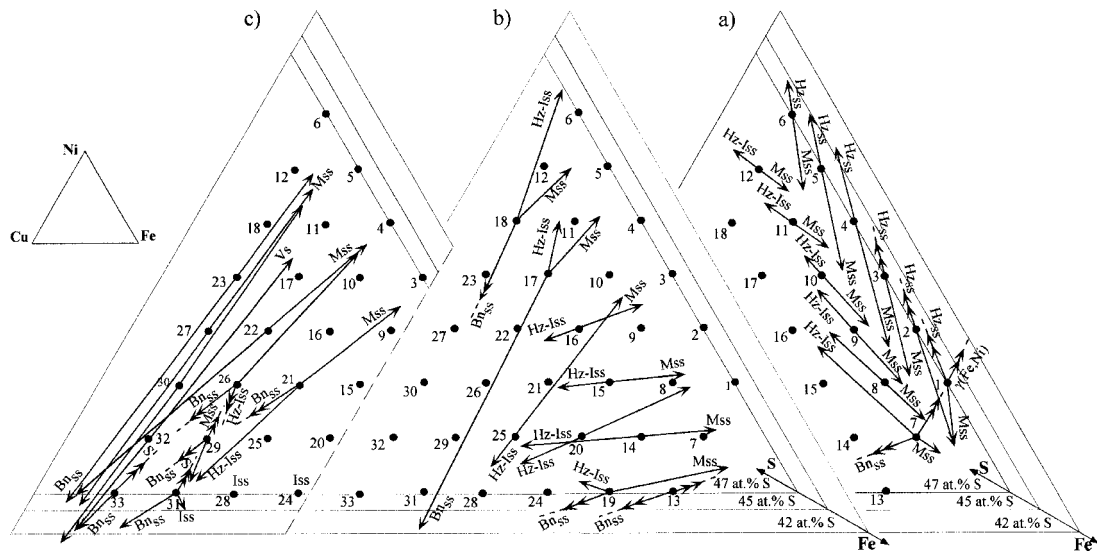
FIG. 5.   Projection of tie-lines joining the compositions of coexisting phases with starting composition of samples with (a) 0–5.9 at.% of Cu, (b) 11.8–23.5 at.% of Cu, (c) 17.7–41.2 at.% of Cu, onto the Fe–Ni–Cu plane of the Fe–Ni–Cu–S tetrahedron. Double arrows with the dashed ends show only the direction in which the composition of the phase is located.

stable, and confirm that Mss is the first liquidus phase to appear during crystallization (Peregoedova 1998). The second phase to be formed is Hz–Iss in the temperature interval 873°–795°C, as indicated by DTA. For Ni-poor or Ni-free samples (charges 20 and 24, respectively), but richer in Cu than the previous ones ($0.33 \leq$ Cu# ≤ 0.44), Hz–Iss appears at a higher temperature, 908° and 877°C, respectively, after crystallization of Mss. The order of appearance of phases is confirmed by the texture of the samples and by the liquidus temperature determined for samples 20 and 24 (962° and 937°C, respectively). Hence, in the Fe-rich and Ni-rich parts of the section Me_9S_8, Hz–Iss occurring in the associations Hz–Iss + Mss ± γ(Fe,Ni) ± Bn$_{ss}$, Hz–Iss + Ni-Mss + Bn$_{ss}$, and Mss + Hz–Iss (see Figs. 1b, 2a, 5ab) is considered to have formed by a peritectic reaction between the early-formed Mss and the residual sulfide liquid. In light of the previous experimental results, therefore, the Hz–Iss solid-solution crystallizes from about 908°C for the starting composition lying in the system Cu–Fe–S down to 806°C for the composition relevant to the system Fe–Ni–S.

In the present experiments, samples with a Cu-rich starting composition (Cu# ≥ 0.44) contain at 760°C a Cu-rich Hz–Iss (33–37 at.% Cu) exsolved from Bn$_{ss}$. For example, sample 26 (Cu# = 0.44) contains the assemblage Hz–Iss + Ni-Mss + Bn$_{ss}$, with Hz–Iss occurring in the matrix of Bn$_{ss}$ as elongate lamellar grains (Fig. 6e). At a higher temperature (870°C), Hz–Iss disappears, and only Mss is stable, together with Bn$_{ss}$ and

liquid. In sample 29, the richest in Cu (Cu# = 0.55), a Cu-rich Hz–Iss reappears as a liquidus phase together with Bn$_{ss}$ and liquid at 870°C. At 840°C, Mss joins Hz–Iss, Bn$_{ss}$ and a S-poor liquid. The approximate composition of the last droplets of the residual liquid in experiments with 0.5 wt% of Pt and Pd added to the starting composition is as follows: 14.4 at.% Fe, 8 at.% Ni, 31 at.% Cu, 44.9 at.% S, 0.6 at.% Pt and 1.1 at.% Pd. At 760°C, no more liquid is present, and the textural relationships of Mss, Hz–Iss and Bn$_{ss}$ (Fig. 1b, diagram IV, Figs. 2a, 5c) confirm an early crystallization of Hz–Iss followed by precipitation of Mss and Bn$_{ss}$. Therefore, in the part of the Me_9S_8 section showing the highest Cu content and a low Ni content, direct crystallization of a Cu-rich Hz–Iss could occur, simultaneously with Mss, or even before Mss and Bn$_{ss}$.

Monosulfide solid-solution (Fe,Ni)$_{1\pm x}$S

Monosulfide solid-solution (Mss) is present in nearly all experimental runs except in Cu-rich samples along the join Fe$_9$S$_8$–Cu$_9$S$_8$ or in those having very low Ni content (*e.g.*, run 32: 35.3 at.% Cu, 5.9 at.% Ni). The shape of the grains of Mss and their textural relationships indicate direct and, in most cases, first-phase crystallization from the sulfide melt (Fig. 4). Subsolidus exsolution-induced lamellae of pentlandite commonly occur in Mss, and their formation is explained by the reduction of the compositional field of Mss upon cooling (Naldrett & Kullerud 1967, Naldrett *et al.* 1967). At
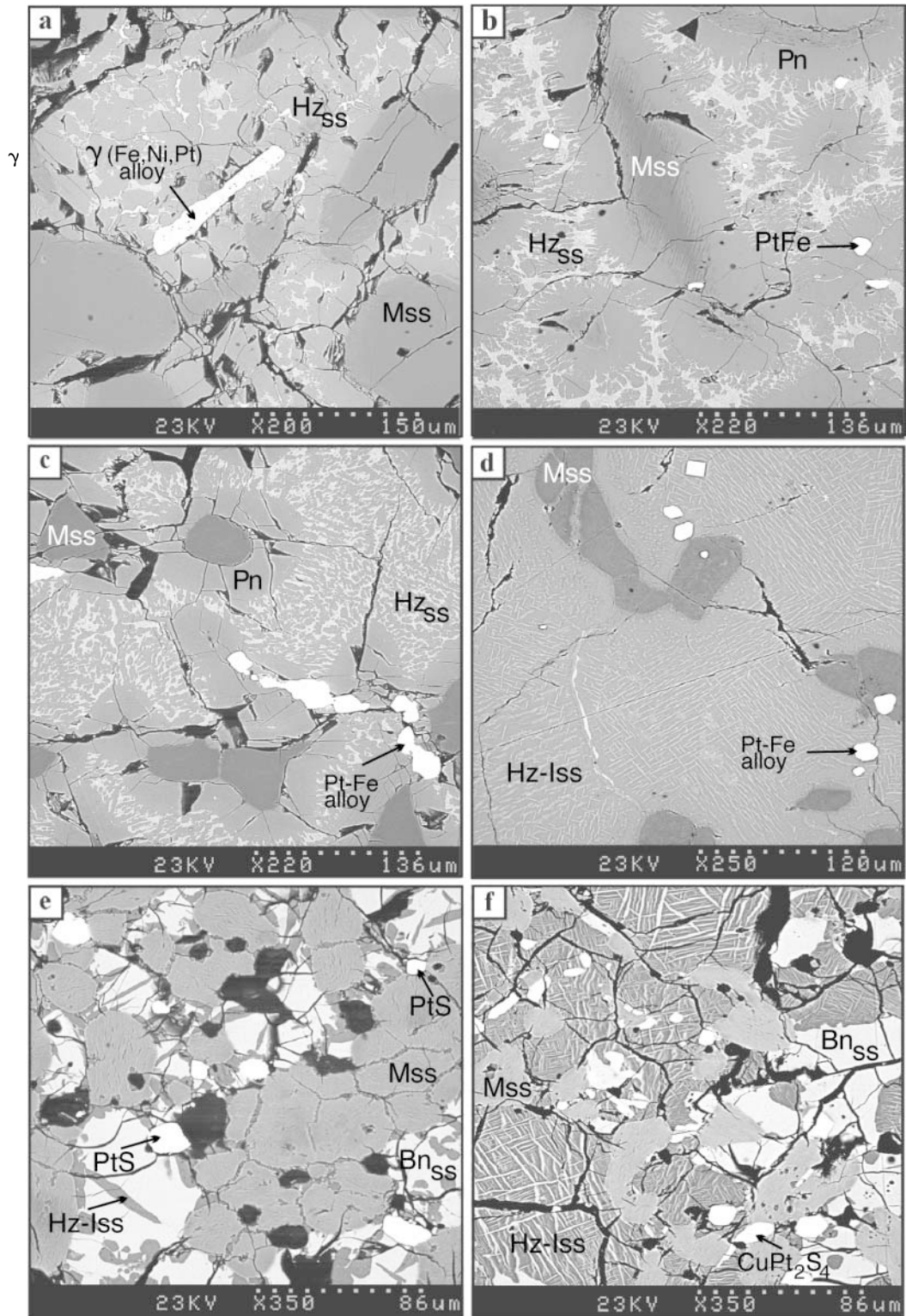
760°C, Mss forms a complete solid-solution between $Fe_{1-x}S$ and $Ni_{1-x}S$, with a Cu content varying from 0.7–1.6 at.% in samples with a low initial Cu content (5.9 at.%), to 2.5–4.6 at.% in samples having bulk Cu ≥ 23.5 at.% (Table 2). The Cu-rich Mss contains many thin sinuous exsolution-induced blebs of Cu-rich phases formed during quenching (Figs. 6e, f). In addition, such Cu-rich Mss is S-rich (51.8–52.1 at.% S) and extremely Ni-rich (31.8–32.9 at.%). Ni,Cu,S-rich Mss seems to have crystallized later than Bn_{ss} or Cu-rich Hz–Iss. In sample 29 (Cu-rich), the crystallization of Cu-rich Hz–Iss followed by Mss is confirmed by experiments conducted at higher temperature (840°C). However, in the 760°C experiment, Mss seems to have been replaced by reaction products formed between Mss and Hz–Iss upon quenching. The phase replacing Mss is very rich in Cu (10.3 at.%) and relatively poor in S (48.6 at.%). A similar composition is also found in experiments with PGE added. Such compositions approach Ni-rich Hz–Iss or Cu-bearing pentlandite (Distler *et al.* 1988). The nearly complete replacement of early-formed Mss could has been favored by the low amount of Mss formed in Cu-rich charges. Relics of Mss enclosed within large rims of a Cu-rich reaction product have been found in experiments on compositions richer in S, with metal proportions close to those of sample 29. This complementary experiment strongly supports the suggestion that Mss is a stable phase in the Cu-rich part of the Me_9S_8 section at 760°C despite its rapid replacement upon quenching. Additional experiments need to be performed in this Cu-rich part of the diagram to better define the liquidus relationships.

FIG. 6. Back-scattered electron images. (a) Elongate grain of primary Pt-bearing γ(Fe,Ni) alloy associated with Mss and Hz_{ss}. Hz_{ss} is present as the quench-decomposition mixture of Pn (grey) with Hz (light grey) and γ(Fe,Ni) alloy (white sinuous exsolution-induced domains) (Pt-containing sample 1 after quenching from 760°C). (b) Grains of Pt–Fe alloy with composition close to natural tetraferroplatinum (PtFe) in association with Mss and Hz_{ss} decomposed as Pn (grey) and fine mixture of heazlewoodite with γ(Fe,Ni) alloy and probably godlevskite. The reaction rims of Pn are located along the contacts between Mss and Hz_{ss} (Pt-containing sample 3 after quenching from 760°C). (c) Pt–Fe alloy with composition intermediate between PtFe and Pt_3Fe. BMS association is similar to that of Pt-containing sample 3 (Fig. 6b) (Pt-containing sample 5 after quenching from 760°C). (d) Euhedral crystals of Pt–Fe alloy coexisting with Cu-rich quaternary solid-solution (decomposed phase) and Mss (Pt-containing sample 20 after quenching from 760°C). (e) Primary crystals of synthetic cooperite (PtS) associated with Mss, Bn_{ss} (light phase) and quaternary solid-solution (dark grey elongate grains in Bn_{ss} matrix). Black spots are polishing defects (Pt-containing sample 26 after quenching from 760°C). (f) Synthetic malanite ($CuPt_2S_4$) in association with Mss (light grey rounded decomposed grains), Hz–Iss (lamellar phase) and Bn_{ss} (Pt-containing sample 29 after quenching from 760°C).

Bornite solid-solution $Cu_{5±x}Fe_{1±y}S_4$

Two kinds of bornite solid-solution (Bn_{ss}) are stable in the Cu-bearing charges of the Me_9S_8 section: (1) primary crystals and (2) large secondary exsolution-induced lamellae or droplets in Hz–Iss. Primary Bn_{ss} (Fig. 2a) crystallizes directly from the sulfide liquid where the Cu content of the system reaches approximately either 15 at.% Cu (at bulk Ni ≥ 11.8 at.%, samples 21–23, 26, 27, 30) or 25–30 at.% Cu (at lower initial Ni content 5.9 at.%, sample 29). Primary Bn_{ss} is associated with Ni-rich Mss or vaesite (Fig. 1b, diagram V) or Ni-rich Mss and Cu-rich Hz–Iss (Fig. 1b, diagram IV; Fig.2a, Table 2). In the association Mss + Bn_{ss} corresponding to the initially Ni-rich part of the Me_9S_8 section, small droplets of Mss generally exsolved from Bn_{ss} upon quenching (Fig. 2a). Similarly, in Cu-rich experiments, quench lamellae of Iss appeared in Bn_{ss} during quenching (samples 31–33). Secondary Bn_{ss} is generally present as coarse droplets or lamellae within the Hz–Iss. In the Fe-rich part of the section showing the association Fe-Mss + Hz–Iss + Bn_{ss} + γ(Fe,Ni) (Fig. 1b, diagrams I and II, Fig. 2a), secondary Bn_{ss} occurs as large exsolution-induced lamellae in the matrix of Hz–Iss. In the Ni-rich part of the section (Ni ≥ 23.5 at.%), containing the association Ni-Mss + Ni-Hz–Iss + Bn_{ss} (samples 17–18, Fig. 2a), Bn_{ss} occurs as large droplet-like grains in close spatial association with Hz–Iss. Finally, Bn_{ss} is also present as quench product and occurs as very small droplets or lamellae within Hz–Iss in almost all of the samples studied.

At 760°C, Bn_{ss} shows a wide range of compositions (Table 2). Both primary and secondary Bn_{ss} are significantly richer in Fe (10.9 ≤ Fe at.% ≤ 15.3) and S (39.9 ≤ S at.% ≤ 43.5) than quench Bn_{ss} (Fe ≤ 3.3 at.%; 33.9 ≤ S at.% ≤ 34.4). The Ni-content of the stable Bn_{ss} does not usually exceed 1.7–2 at. %, but in the sample richest in Ni containing primary Bn_{ss} and Mss (sample 23), it can reach 4 at.%.

Vaesite $(Ni,Fe)S_2$

Vaesite (Vs) was obtained in only one sample in the Cu-rich part of the Me_9S_8 section, in association with Bn_{ss}. The shape of the grains of vaesite is indicative of its direct crystallization from the sulfide melt, but after primary crystallization of Bn_{ss}. Such vaesite contains significant amounts of Fe (2 at.%) and Cu (6.3 at.%) in solid solution.

γ(Fe,Ni) alloy

The alloy γ(Fe,Ni) occurs as rounded or irregularly shaped grains in association with Mss and Hz_{ss} in the Fe-rich part of $Fe_9S_8 – Ni_9S_8$ join of the Me_9S_8 section or together with Mss, Hz–Iss and Bn_{ss} in the Cu-bearing assemblages. The sinuous or droplet-shaped exsolution-induced blebs of γ(Fe,Ni) are very common

in the quenched mixture of the Fe-rich heazlewoodite or quaternary solid-solutions.

Phase equilibria in the Me_9S_8 section at 760°C

The construction of an accurate diagram of phase relationships in the Me_9S_8 section is very complicated because it intersects two-, three- and four-phase assemblages stable in the central part of system Fe–Ni–Cu–S with phase compositions lying outside the planar Me_9S_8 section (Fig. 1). The precise position of the boundary between the various assemblages stable in the Me_9S_8 section would require a large number of additional experiments; therefore, the domains of their stability are projected only schematically onto the Me_9S_8 section (Fig. 2a).

The two-phase association of Mss and Hz–Iss dominates the central part of the Me_9S_8 section at 760°C. A three-phase field with Mss + Hz–Iss + Bn$_{ss}$ is located on each side of the two-phase Mss + Hz–Iss area, one developed from an Fe-rich starting composition and the second one emanating from a Ni- and Cu-rich composition. The boundary of the three-phase assemblage in the Fe-rich part of the Me_9S_8 section is only approximately located owing to insufficient experimental data. Boundaries of other fields drawn in the Fe-rich part of the Me_9S_8 section are also tentative for the same reasons [Mss + Bn$_{ss}$, Mss + Hz$_{ss}$ + γ(Fe,Ni), Mss + Hz–Iss + Bn$_{ss}$ + γ(Fe,Ni)]. Four associations [Mss + γ(Fe,Ni), Mss + γ(Fe,Ni) + Bn$_{ss}$, Mss + Bn$_{ss}$ + γ(Fe,Ni) + αFe and Mss + Bn$_{ss}$ + αFe] were not covered by our experiments, but their presence in this section can be predicted from both the literature data on the bounding systems Fe–Ni–S and Cu–Fe–S (Kullerud *et al.* 1969, Cabri 1973) and the logical arrangement of stability fields in the phase diagram.

In the second three-phase field [Mss + Hz–Iss + Bn$_{ss}$], the composition of phases, notably that of Hz–Iss, gradually changes in response to changes in starting composition. However, there is a small area in which uncertainty exists in phase relations (grey area, Fig. 2a). Within this small region, the composition of Hz–Iss abruptly changes from Ni-rich (samples 17 and 18) to Cu-rich (samples 21, 26 and 29; Figs. 5b, c). Variation in the chemical composition of Hz–Iss is accompanied by the change in the shape and texture of the grains, which is indicative of distinct modes of formation. Three modes are distinguished: (1) in the Ni-rich samples (sample 17), Ni-rich Hz–Iss forms by a peritectic reaction of sulfide liquid with monosulfide solid-solution (Table 2); (2) in Ni-poor and Cu-rich samples (sample 26), Cu-rich Hz–Iss is a subsolidus phase that exsolved from bornite solid-solution (Fig. 6e); (3) in sample 29, the richest in Cu, Hz–Iss is a liquidus phase that crystallized directly from a Cu-rich liquid. More detailed experimental work will have to be done for a range of starting compositions intermediate between the above

samples in order to determine precisely where conditions of crystallization of Hz–Iss change and what is their bearing on the phase relationships. Nevertheless, the proposed shape of the field [Mss + Hz–Iss + Bn$_{ss}$] appears reliable, since it reflects the shape of the compositional field of the quaternary solid-solution (Figs. 1a, 3a). The abrupt change in Hz–Iss composition within the "uncertain region" in the field [Mss + Hz–Iss + Bn$_{ss}$] is due to a very steep, almost perpendicular position of tie-lines connecting the compositions of monosulfide and quaternary solid-solutions.

A large two-phase association of Ni-rich Mss and Bn$_{ss}$ exists in the Cu- and Ni-rich part of the Me_9S_8 section. The phase assemblage of vaesite with bornite solid-solution represents the tie-lines connecting Vs and Bn$_{ss}$ in the three-phase volume Vs + Bn$_{ss}$ + S$_L$, which is traversed in the Cu-rich part of the Me_9S_8 section (Fig. 5c). The three other Vs-bearing associations [Mss + Bn$_{ss}$ + Vs; Mss + Bn$_{ss}$ + Vs + Hz–Iss; Bn$_{ss}$ + Vs + Hz–Iss + S$_L$] were not encountered in this study, but they should appear in the Cu-rich part of the Me_9S_8 section (Fig. 2a) according to the predicted equilibrium fields in the phase diagram. Two associations, Bn$_{ss}$ + S$_L$ and Bn$_{ss}$ + Iss + S$_L$, obtained for Cu-rich compositions along the Fe$_9S_8$ – Cu$_9S_8$ join, are in agreement with results of previous studies of the system Cu–Fe–S (Kullerud *et al.* 1969, Cabri 1973). These fields probably extend inward to the Fe–Ni–Cu–S tetrahedron because Ni is able to enter both Iss and Bn$_{ss}$ solid-solutions.

PGM ASSEMBLAGES IN PGE-BEARING EXPERIMENTS IN THE SYSTEM Fe–Ni–Cu–S

The chemical composition of platinum-group minerals (PGM) and the major sulfide solid-solutions in the experiments in which minor amounts of Pt, (Pt+Pd), Pd, and Rh (1 wt.%) were added is summarized in Tables 3 to 6. The minerals that concentrate PGE are presented in Table 7, together with the base-metal sulfide (BMS) associations. At constant sulfur content, the starting proportions of the base metals (Fe, Ni and Cu) control the formation of the different PGE-phases. Platinum, in particular, forms distinct phases as Ni and Cu contents increase in the system. The metal:S ratio of BMS was not affected by addition of PGE.

Platinum

Pt forms Pt–Fe alloys in association with Fe-rich base-metal sulfides or platinum sulfides in Ni- and Cu-rich assemblages (Fig. 2b). The morphology of Pt-bearing phases is usually characterized by well-developed crystal faces, testifying to their direct crystallization from a sulfide liquid, commonly before the crystallization of Mss (Fig. 6). The Pt content of the base-metal sulfide solid-solutions was generally found to be below the detection limit of electron-microprobe approach

(Table 3), except in the Cu-rich part of the section, where the Pt content of Mss reaches 0.1 at.%. The successive Pt phases observed in BMS associations as Fe decreases are as follows (Fig. 2b, Table 3):

(1) Pt-rich γ(Fe,Ni) alloys occur together with Mss and Hz$_{ss}$ (Fig. 6a) from the most Fe-rich initial bulk-composition [Fe/Cu ≥ 7]. Up to 10.0 at.% Pt is found in the γ(Fe,Ni) alloy. Natural Ni–Fe alloys like awaruite,

TABLE 3. REPRESENTATIVE RESULTS OF EXPERIMENTS IN Pt-CONTAINING SECTION Me$_9$S$_8$ OF THE Fe-Ni-Cu-S SYSTEM AT 760°C.

N°	log f(S₂)	BMS association	Chemical composition						Coexisting Pt phase	Composition of Pt phase						Chemical formulae of Pt phase
			Fe	Ni	Cu	Pt	S	Σ		Fe	Ni	Cu	Pt	S	Σ	
1	-10.5	Fe-Mss	59.3*	3.5	0	n.d.**	36.7	99.5		32.5	39.5	0	27.3	0.1	99.4	-
			46.8	2.6	0		50.5		γ(Fe,Ni,Pt)							
		Hz$_{ss}$	31.5	35.8	0	n.d.	32.3	99.7		41.6	48.2	0	10.0	0.1		
			25.9	27.9	0		46.2									
2	-7.5	Fe-Mss	52.8	10.2	0	n.d.	36.6	99.5		17.7	5.5	0	76.2	0.1	99.5	Pt$_{0.97}$Fe$_{0.79}$Ni$_{0.23}$
			41.8	7.7	0		50.5									
		Hz$_{ss}$	29.0	39.9	0	n.d.	30.7	99.7		39.3	11.6	0	48.5	0.5		
			24.1	31.5	0		44.4									
3	-6.2	Fe-Mss	47.0	15.8	0	n.d.	37.0	99.9		15.8	6.2	0	77.9	0.1	100.1	Pt$_{1.01}$Fe$_{0.71}$Ni$_{0.27}$
			37.2	11.9	0		51.0									
		Hz$_{ss}$	24.5	45.1	0	n.d.	30.9	100.5		35.7	13.4	0	50.4	0.4		
			20.2	35.4	0		44.4									
15	-5.5	Fe-Mss	46.1	13.9	3.5	n.d.	36.0	99.6		14.5	4.2	2.69	79.9	0.1	101.4	Pt$_{1.04}$Fe$_{0.66}$Ni$_{0.18}$Cu$_{0.1}$
			36.9	10.6	2.5		50.1									
		Hz-Iss	31.0	14.0	23.2	n.d.	31.4	99.6		33.0	9.0	5.38	52.1	0.5		
			26.0	11.1	17.1		45.8									
5	-4.4	Mss	30.3	33.3	0	n.d.	36.9	100.5		10.1	2.1	0	87.9	0.1	100.2	-
			24.0	25.1	0		50.9									
		Hz$_{ss}$	17.0	51.4	0	n.d.	32.0	100.6		27.0	5.3	0	67.1	0.5		
			14.0	40.1	0		45.8									
10	-4.6	Fe-Mss	36.8	23	5.3	n.d.	35.1	99.8		10.3	1.7	0.71	87.8	0.1	100.7	-
			29.7	17	3.8		49.3									
		Hz-Iss	25.8	31	11.4	n.d.	31.5	99.7		27.2	4.3	1.64	66.3	0.6		
			21.4	25	8.3		45.7									
20	-4.6	Fe-Mss	45.6	11.5	7.7	n.d.	34.6	99.4		9.8	0.4	0.97	89.8	0.1	101.1	-
			36.9	8.8	5.5		48.8									
		Hz-Iss	31.6	5.9	30.6	n.d.	31.1	99.2		26.4	1.1	2.30	69.5	0.7		
			26.7	4.8	22.8		45.8									
22	-3.6	Ni-Mss	24.3	35.5	4.1	0.1	35.5	99.6		0.2	1.7	0.68	85.1	13.9	101.5	Pt$_{0.96}$Ni$_{0.06}$Cu$_{0.02}$Fe$_{0.01}$S$_{0.95}$
			19.7	27.3	2.9	0.02	50.1		PtS							
		Bn$_{ss}$	15.8	0.2	56.0	n.d.	28.1	100.2		0.5	3.1	1.17	47.9	47.4		
			13.8	0.2	43.1		42.9									
26	-1.7	Ni-Mss	25.2	32.3	5.4	0.55	36.1	99.5		0.3	1.4	1.04	84.8	14.4	102.0	Pt$_{0.93}$Ni$_{0.05}$Cu$_{0.04}$Fe$_{0.01}$S$_{0.97}$
			20.4	24.8	3.8	0.13	50.9		PtS							
		Hz-Iss***			no data											
		Bn$_{ss}$	14.6	0.4	57.8	n.d.	27.5	100.3		0.6	2.6	1.75	46.7	48.4		
			12.9	0.3	44.7		42.1									
27	-1.1	Ni-Mss	15.3	44.3	3.3	0.47	37.2	100.7		1.7	8.4	12.1	54.0	26.2	102.4	Cu$_{0.92}$Pt$_{1.33}$Ni$_{0.69}$Fe$_{0.15}$S$_{3.93}$
			12.2	33.6	2.3	0.11	51.7		CuPt$_2$S$_4$							
		Bn$_{ss}$	13.7	0.4	57.8	n.d.	27.0	98.8		2.1	9.8	13.1	19.0	56.1		
			12.2	0.4	45.4		42.0									
29	>0	Ni-Mss			no data											
		Hz-Iss	27.1	2.2	36.9	n.d.	33.3	99.6		2.9	7.0	14.0	52.4	26.3	102.6	Cu$_{1.04}$Pt$_{1.27}$Ni$_{0.56}$Fe$_{0.25}$S$_{3.88}$
			22.6	1.8	27.1		48.5		CuPt$_2$S$_4$							
		Bn$_{ss}$	13.2	0.2	60.5	n.d.	26.3	100.2		3.5	8.0	14.9	18.2	55.4		
			11.8	0.1	47.3		40.7									

* For each phase, compositions expressed in wt.% are in the first row, in at.% - in the second row; the starting compositions of the samples are given in the Table 2.

** Here and elsewhere in the article, "n.d." means "below limit of detection for PGE".

*** One of quench products of Hz-Iss was analyzed: in wt.% Fe(29), Ni(3.2), Cu(32.7), S(34.4), Σ(99.3); in at.% Fe(24), Ni(2.5), Cu(23.8), S(49.7).

TABLE 4. RESULTS OF EXPERIMENTS IN Pd-CONTAINING SECTION Me_9S_8
OF THE SYSTEM Fe-Ni-Cu-S AT 760°C.

N°	log $f(S_2)$	BMS association	Chemical composition						Coexisting Pd phase	Composition of Pd phase						Chemical formulae of Pd phase
			Fe	Ni	Cu	Pd	S	Σ		Fe	Ni	Cu	Pd	S	Σ	
7	-10.5	Fe-Mss	59.0*	2.2	2.0	n.d.	36.0	99.3	γ(Fe,Ni,Pd)	28.2	35.9	7.8	29.4	0.3	101.6	-
			47.0	1.7	1.4		49.9									
		Hz-Iss	34.1	17.9	16.7	0.4	29.9	99.0		33.1	40.1	8.1	18.1	0.6		
			28.9	14.4	12.4	0.2	44.1									
13**	-	Po_ss	60.4	0	3.5	n.d.	36.5	100.4	Pd(Cu,Fe)	13.8	0	22	66.2	0	101.7	$Pd_{1.03}Cu_{0.56}Fe_{0.41}$
			47.5	0	2.4		50.0									
		Bn_ss	17.2	0	57.1	n.d.	27.3	101.6		20.5	0	28	51.3	0		
			14.9	0	43.7		41.4									
Pd scatters in the base-metal sulfide solid-solutions (BMS)									*Pd content of Mss (at.%)*				*Pd content of Hz-Iss (at.%)*			
4	-5.7	Fe-Mss	42.9	19.3	0	n.d.	36.4	98.7		*very low*				0.5		
			34.4	14.7	0		50.8									
		Hz_ss***	23.0	45.4	0	1.1	30.7	100.2								
			19.1	35.9	0	0.5	44.4									
5	-4.4	Ni-Mss	25.1	38.3	0	0.3	36.3	100.0		0.1				1.0		
			20.1	29.2	0	0.1	50.6									
		Hz_ss***	14.5	52.5	0	2.3	30.9	100.4								
			12.2	41.7	0	1.0	45.0									
6	-4.1	Ni-Mss	22.8	40.8	0	0.12	36.3	99.9		0.05				*no data*		
			18.2	31.1	0	0.05	50.6									
		Hz_ss	*no data*													
10	-4.6	Fe-Mss	41.6	19.8	2	0.11	36.6	99.8		0.05				0.5		
			33.1	15.0	1	0.05	50.7									
		Hz-Iss***	24.9	29.0	13.1	1.2	31.6	99.7								
			20.8	23.0	9.7	0.5	46.0									
11	-4.1	Ni-Mss	29.9	32.4	1.4	0.08	36.8	100.6		*very low*				0.6		
			23.7	24.4	1.0	0.03	50.8									
		Hz-Iss	19.7	38.0	8.7	1.3	32.3	100.1								
			16.4	30.0	6.4	0.6	46.7									
12	-3.7	Ni-Mss	*no data*							*no data*				0.7		
		Hz-Iss	12.5	53.4	2.2	1.7	31.3	101.1								
			10.4	42.1	1.6	0.7	45.2									
		Bn_ss	7.2	1.3	69.8	n.d.	23.7	102.0								
			6.5	1.1	55.2		37.2									
17	-3.7	Ni-Mss	24.6	36.9	2.4	0.2	36.4	100.5		0.1				1.5		
			19.6	28.0	1.7	0.1	50.6									
		Hz-Iss	18.7	37.3	8.6	3.3	32.2	100.2								
			15.7	29.7	6.3	1.5	46.9									
		Bn_ss	14.6	0.3	57.9	n.d.	27.9	100.7								
			12.8	0.3	44.5		42.4									
20	-4.6	Fe-Mss	49.0	9.8	3.9	0.1	36.1	98.9		*very low*				0.2		
			39.3	7.4	2.7	0.04	50.4									
		Hz-Iss	31.7	4.2	30.2	0.5	31.7	98.3								
			26.9	3.4	22.6	0.2	46.9									
25	-2.8	Mss	*no data*							*no data*				0.5		
		Hz-Iss	28.1	7.3	32.9	1.0	31.2	100.4								
			23.6	5.8	24.4	0.5	45.7									
*Pd scatters in BMS with (Pd,Cu,Ni,Fe)S**** exsolving during their quenching from 760°C*																
26	-1.7	Ni-Mss	27.3	31.1	3.0	2.2	36.7	100.3	-							$Pd_{0.65}Cu_{0.14}Ni_{0.13}Fe_{0.12}S_{0.96}$
			21.9	23.8	2.1	0.9	51.3									
		Hz-Iss	19.0	4.9	44.8	2.0	29.1	99.8		5.6	6.4	7.1	57.1	25.3	101.5	
			16.6	4.1	34.3	0.9	44.1									
		Bn_ss	15.3	0.4	56.6	0.07	27.9	100.3		6.1	6.6	6.8	32.6	47.9		
			13.5	0.3	43.6	0.03	42.6									
28	-1.4	Iss(Cu>Fe)	26.7	0	41.1	0.9	31.0	99.8	-	10.3	0	15.7	50.3	24.7	101.0	$Pd_{0.56}Cu_{0.29}Fe_{0.22}S_{0.92}$
			22.8	0	30.8	0.4	46.0			11.0	0	14.8	28.2	46.0		
29	>0	Mss*****	20.2	28.5	13.5	4.6	33.3	99.9	-	13.1	6.4	19.3	31.6	29.1	99.5	$Pd_{0.32}Cu_{0.33}Ni_{0.12}Fe_{0.25}S_{0.98}$
			16.9	22.7	9.9	2.0	48.5									
		Hz-Iss	25.9	2.7	38.3	0.2	33.1	100.2		12.7	5.9	16.4	16.0	49.0		
			21.6	2.1	28.1	0.1	48.1									
		Bn_ss	*no data*													
30	>0	Ni-Mss	14.6	42.7	3.7	2.7	37.0	100.7	-	3.0	5.7	10.8	57.6	24.4	101.5	$Pd_{0.67}Cu_{0.21}Ni_{0.12}Fe_{0.07}S_{0.94}$
			11.7	32.7	2.6	1.1	51.9									
		Bn_ss	13.3	2.3	58.3	0.3	26.9	101.2		3.4	6.0	10.4	33.4	46.8		
			11.7	1.9	45.0	0.1	41.2									
32	>0	Vs	*no data*							7.7	7.1	16.3	43.5	26.5	101.2	$Pd_{0.47}Cu_{0.29}Ni_{0.14}Fe_{0.16}S_{0.94}$
		Bn_ss	15.2	1.5	56.1	0.5	27.7	100.9		7.9	6.9	14.7	23.3	47.2		
			13.3	1.2	43.1	0.2	42.2									

TABLE 4.   RESULTS OF EXPERIMENTS IN Pd-CONTAINING SECTION Me_9S_8
OF THE SYSTEM Fe-Ni-Cu-S AT 760°C.

N°	$\log f(S_2)$	BMS association	Chemical composition						Coexisting Pd phase	Composition of Pd phase						Chemical formulae of Pd phase
			Fe	Ni	Cu	Pd	S	Σ		Fe	Ni	Cu	Pd	S	Σ	
31	>0	Iss(Cu>Fe)	26.9	0	41.9	0.8	30.8	100.5	*Quench exsolutions of Cu,Fe,Pd-sulfide**** in a matrix of Bnss*							
			22.8	0	31.3	0.4	45.6			16.4	0	33.9	21.6	27.5	99.4	-
		Bn$_{ss}$			*no data*				-	15.6	0	28.2	10.8	45.5		-
33	>0	Bn$_{ss}$******	11.8	0	61.4	n.d.	26.9	100.2		9.2	0	42.1	24.4	26.0	101.7	
			10.5	0	47.9		41.6		-	8.9	0	35.5	12.3	43.4		-

*   For each phase, compositions expressed in wt.% are in the first row, in at.% - in the second row.

**   The starting compositions are given in the Table 2; the starting composition of the sample number 13 (in at.%) is Fe(41.2),
           Ni(0), Cu(11.8), S(47) with 1wt.% of Pd added into the BMS association.

***   Pentlandite exsolved from Hz-Iss upon quenching was analyzed with the use of narrow electron beam (2-3μm).

Sample	28.4	38.5	0	0.3	32.8	100.0	Sample	27.7	36.3	2.3	0.7	32.5	99.6
4	23.3	29.9	0	0.1	46.7		10	22.9	28.5	1.7	0.3	46.7	
5	16.2	48.5	0	2.3	32.7	99.6							
	13.4	38.3	0	1.0	47.3								

****   Because of the small size of the exsolutions of Pd-phase, the BMS matrix might be included in an area analyzed by EPMA.

***** The product of reaction between Mss and Hz-Iss was analyzed.

******Bn$_{ss}$ matrix was analyzed between lamellar exsolutions of Pd-phase with the use of narrow electron beam (2-3 μm).

TABLE 5.   REPRESENTATIVE COMPOSITIONS OF Pt-Pd PHASES STABLE
IN THE Me_9S_8 SECTION AT 760°C.

N°	Pt-Pd phase	Composition of Pt-Pd phase							Chemical formulae of Pt-Pd phase
		Fe	Ni	Cu	Pt	Pd	S	Σ	
7	γ(Fe,Ni,Pt,Pd)	27.6*	18.6	4.1	32.6	16.4	0.1	99.2	-
		41.2	26.4	5.3	14.0	12.8	0.2		
3	Pt-Fe alloys with a composition close to PtFe	15.1	5.3	0	78.1	0.7	0.1	99.3	$Pt_{1.04}Pd_{0.02}Fe_{0.7}Ni_{0.23}$
		35.2	11.7	0	52.0	0.9	0.3		
8		14.5	3.7	2.4	77.6	1.8	0.1	100.1	$Pt_{1.02}Pd_{0.02}Fe_{0.67}Ni_{0.23}$
		33.4	8.0	4.8	51.1	2.2	0.5		
14		17.0	3.1	3.2	75.5	1.7	0.1	100.6	$Pt_{1.04}Pd_{0.04}Fe_{0.7}Ni_{0.16}Cu_{0.1}$
		37.4	6.5	6.2	47.6	1.9	0.4		
4	Pt-Fe alloys with a composition intermediate between PtFe and Pt₃Fe	12.9	4.1	0	81.4	1.1	0.1	99.5	-
		31.6	9.5	0	57.1	1.4	0.4		
17		9.2	1.1	0.9	87.9	0.4	0.1	99.6	-
		25.3	2.8	2.1	68.8	0.6	0.3		
19		12.8	0	1.5	84.4	1.8	0.1	100.6	-
		32.5	0	3.4	61.3	2.4	0.4		
21		9.2	0.6	0.8	89.3	0.6	0.1	100.6	-
		25.1	1.5	1.9	70.1	0.9	0.4		
24		9.5	0	1.0	88.6	1.4	0.1	100.6	-
		25.9	0	2.3	69.2	1.9	0.6		
22	Probably PtS** and Pd in BMS	0.6	2.6	0.7	80.5	3.4	12.4	100.2	-
		1.2	4.9	1.2	46.0	3.5	43.2		
25		1.1	1.2	2.2	79.9	4.7	12.2	101.3	-
		2.2	2.2	3.9	45.0	4.8	41.9		
27	CuPt₂S₄ and Pd in BMS	1.6	7.7	13.1	52.8	0	24.2	99.3	$Cu_{1.03}Pt_{1.36}Ni_{0.66}Fe_{0.14}S_{3.8}$
		2.1	9.4	14.8	19.4	0	54.3		
29		3.0	7.3	13.9	51.3	0.2	24.6	100.2	$Cu_{1.07}Pt_{1.29}Ni_{0.61}Fe_{0.27}Pd_{0.01}S_{3.76}$
		3.8	8.7	15.3	18.4	0.1	53.7		

*   For each phase, compositions expressed in wt.% are in the first row, in at.% - in the second row; the starting compositions of
      the samples are given in the Table 2; 0.5 wt.% of Pt and Pd were added into BMS associations; the BMS associations are the
      same as in the experiments with Pt and Pd.

** The small size of the crystals of Pt-Pd phases does not allow reliable analyzing by EPMA.

TABLE 6.   REPRESENTATIVE RESULTS OF EXPERIMENTS IN Rh-CONTAINING SECTION Me_9S_8 OF THE SYSTEM Fe-Ni-Cu-S AT 760°C.

N°	log $f(S_2)$	BMS association	Chemical composition						Coexisting Rh phase	Composition of Rh phase					
			Fe	Ni	Cu	Rh	S	Σ		Fe	Ni	Cu	Rh	S	Σ
1**	-10.5	Fe-Mss	59.1*	4.54	0	n.d.	36.6	100.3	γ(Fe,Ni,Rh)	34.7	25.7	0	40.4	0.02	100.8
			46.5	3.39	0		50.1								
		Hz$_{ss}$	31.6	35.5	0	n.d.	31.7	98.85		42.8	30.1	0	27.1	0.04	
			26.2	28	0		45.8								
7**	-10.5	Fe-Mss	58.8	2.44	2.31	n.d.	35.9	99.48	FeRh	35.2	4.34	1.31	59.3	0.02	100.2
			46.8	1.84	1.62		49.7								
		Hz-Iss	34	19	16	n.d.	31	100		48.4	5.67	1.58	44.3	0.04	
			28.3	15	11.8		44.9								
3	-6.2	Fe-Mss	47.3	15.3	0	1.37	36.2	100.2	*Rh scatters in BMS*						
			37.6	11.5	0	0.59	50.2		Rh content of M$_{ss}$	Rh content of Hz-Iss (at.%)					
		Hz$_{ss}$***	25.9	42.4	0	0.46	31.4	100.2	0.59	0.21					
			21.4	33.3	0	0.21	45.2								
4	-5.7	Fe-Mss	39.7	22.1	0	1.61	36.5	99.95	0.7	0.24					
			31.7	16.8	0	0.7	50.8								
		Hz$_{ss}$***	23.4	44.1	0	0.54	31.9	100							
			19.3	34.6	0	0.24	45.9								
5	-4.4	Ni-Mss	30.3	32.2	0	1.97	36.6	101.1	0.85	0.2					
			24.1	24.3	0	0.85	50.7								
		Hz$_{ss}$***	16.9	51.1	0	0.45	31.5	99.96							
			14	40.2	0	0.2	45.5								
9	-5.7	Fe-Mss	46	13.6	2.39	1.7	35.8	99.41	0.74	0.15					
			37	10.4	1.69	0.74	50.2								
		Hz-Iss***	28.7	28.8	10.7	0.33	31.1	99.65							
			23.9	22.9	7.85	0.15	45.2								
13	-	Po$_{ss}$	57.8	0	4.1	1.62	35.8	99.34	0.71	-					
			46.3	0	2.89	0.71	50								
		Bn$_{ss}$	16.6	0	56.9	n.d.	26.7	100.3							
			14.7	0	44.2		41.1								
14	-6.8	Fe-Mss	54	5.51	2.92	1.64	36	100	0.71	*very low*					
			43.1	4.18	2.05	0.71	50								
		Hz-Iss***	29.4	10.7	29.4	n.d.	30	99.48							
			25	8.62	21.9		44.5								
15	-5.5	Fe-Mss****	44.2	13.4	5.13	2.04	35.2	100	0.89	0.06					
			35.7	10.3	3.64	0.89	49.5								
		Hz-Iss	29.6	16.2	22.2	0.13	31.8	99.87							
			24.6	12.8	16.3	0.06	46.2								
19	-5.7	Po$_{ss}$	55.5	0	5.11	2.14	36.9	99.63	0.93	*very low*					
			44.3	0	3.58	0.93	51.2								
		Iss***	38.3	0	26.9	n.d.	33.7	98.9							
			31.8	0	19.6		48.6								
21	-3.7	Fe-Mss	35.1	22.7	4.79	1.98	34.8	99.3	0.88	*no data*					
			28.6	17.6	3.44	0.88	49.4								
		Hz-Iss , Bn$_{ss}$	*no data*												
23	-3.1	Ni-Mss	15.1	46	2.48	1.62	35.7	101	0.71	-					
			12.2	35.2	1.76	0.71	50.1								
		Bn$_{ss}$*****	*no data*												
25	-2.8	Fe-Mss	34.5	19.8	3.71	5.82	35.3	99.15	2.6	*very low*					
			28.4	15.5	2.69	2.6	50.8								
		Hz-Iss	27.6	3.52	37.4	n.d.	30.7	99.22							
			23.5	2.85	28		45.6								

TABLE 6. REPRESENTATIVE RESULTS OF EXPERIMENTS IN Rh-CONTAINING SECTION Me_9S_8 OF THE SYSTEM Fe-Ni-Cu-S AT 760°C.

N°	log $f(S_2)$	BMS association	Fe	Ni	Cu	Rh	S	Σ	Coexisting Rh phase	Fe	Ni	Cu	Rh	S	Σ
27	-1.1	Ni-Mss	14.3	42.9	4.29	2.09	36.3	99.79	0.92				-		
			11.6	33.1	3.07	0.92	51.3								
		Bn$_{ss}$	13.6	0.53	59	n.d.	26.4	99.63							
			12.1	0.45	46.3		41.1								
29	>0	Mss******	24.3	31.2	9.88	0.22	34.4	100.1	0.1				-		
			19.8	24.2	7.07	0.1	48.8								
		Bn$_{ss}$*****, Hz-Iss			no data										
28	-1.4	Iss	27.2	0	41.4	n.d.	30.9	99.49	CuRh$_2$S$_4$	11.7	0	13.4	43.9	32.6	101.7
			23.2	0	31		45.8			11.2	0	11.3	22.9	54.5	
32	>0	Vs	3.29	42.4	2.61	n.d.	52.1	100.4	(Rh,Ni)S$_2$	1.43	14	5.34	34.2	45.4	100.4
			2.41	29.5	1.68		66.4			1.22	11.4	4.01	15.8	67.6	
		Bn$_{ss}$*****			no data										

* For each sample, compositions expressed in wt.% are in the first row, in at.% - in the second row; the starting compositions of the samples are given in the Table 2.

** The γ(Fe,Ni) alloy exsolved from Hz-Iss upon quenching and formed a rim around primary Rh-phase:

Sample 1	28.5	69.7	0	0.05	0.2	98.44	Sample 7	34.1	60.9	3.2	0.9	0.04	99.1
	30	69.6	0	0.03	0.37			35.7	60.8	2.9	0.5	0.1	

*** The quench products of Hz-Iss were analyzed with the use of narrow electron beam (2-3 μm):

Sample 3	Pn	33.8	32.4	0	0.81	33	100	Hz	14.2	57.8	0	0.04	28.9	101
		27.6	25.2	0	0.36	46.9			11.9	46	0	0.02	42.1	
4	Pn	28.6	37.4	0	1.2	33	100.3	Hz	10.9	60.8	0	n.d.	28.9	100.7
		23.4	29.1	0	0.53	47			9.12	48.6	0		42.3	
5	Pn	25.3	40	0	1.68	32.7	99.73	Hz	8.91	63.1	0	n.d.	29	101.1
		20.9	31.4	0	0.75	47			7.45	50.2	0		42.3	
9	Pn	35.5	28.1	2.34	1.68	33	100.7							
		28.9	21.8	1.67	0.74	46.9								
14	Pn	40.1	23.3	4.03	n.d.	32.7	100.1	Hz	32.3	15	22.7	0.05	30.5	100.5
		32.7	18.1	2.89		46.4			27	11.9	16.7	0.02	44.5	

**** The reactional border of Pn between the grains of Mss and Hz-Iss was analyzed: in wt.% Fe(35.3), Ni(27.8), Cu(3.03), Rh(1.58), S(32.7), Σ(100.4); in at.% Fe(28.9), Ni(21.6), Cu(2.18), Rh(0.7), S(46.6).

***** The Bn matrix of Bn$_{ss}$ was analyzed with the use of narrow electron beam (2-3 μm).

Sample 23	12.3	0.64	61.7	n.d.	26	100.6	Sample 32	12.7	0.22	60.7	n.d	26.4	100.1
	10.9	0.54	48.3		40.2			11.3	0.18	47.5		41	
29	18.8	2.12	49.1	n.d.	28.9	98.89							
	16.4	1.76	37.7		44.1								

****** The product of reaction between Mss and Hz-Iss was analyzed.

which are considered to be secondary minerals formed during serpentinization, can also host significant amounts of PGE (Ahmed & Bevan 1981, Augé et al. 1999).

(2) For slightly less Fe-rich compositions (2.5 ≤ Fe/Cu ≤ 6), a Pt–Fe alloy with a composition corresponding to tetraferroplatinum (PtFe) appears with Mss and Hz–Iss that are richer in Ni than those from very Fe-rich compositions like (1) above (Fig. 6b). Significant amounts of Ni and Cu are present in the Pt–Fe alloy. The maximum Ni (up to 13 at.%) and Cu (up to 5 at.%) was measured in alloys associated with Ni- and Cu-rich BMS. In natural PGE deposits, tetraferroplatinum may show extensive solid-solutions with Rh, Pd, Ni and Cu (Cabri et al. 1996). Complete solid-solution between tetraferroplatinum and tulameenite (Pt$_2$FeCu) exists in nuggets from ophiolitic placers (Augé et al. 1998), and alloys with a composition intermediate between ideal tulameenite and hypothetical Pt$_2$FeNi are described from the Onverwacht mine (Cabri et al. 1977).

(3) In most of the central part of the Me_9S_8 section (1.25 < Fe/Cu < 4, Figs. 6c, d), a Pt–Fe alloy containing between 60 and 70 at.% Pt and up to 10 at.% Ni is stable with Mss and Hz–Iss showing a variable Fe:Ni ratio (± Bn$_{ss}$). The composition of the Pt–Fe alloy [1.5 ≤ PGE/BM ≤ 2.5; PGE/BM = (Pt+Pd)/(Fe+Ni+Cu)] is intermediate between that of tetraferroplatinum (PtFe) and isoferroplatinum (Pt$_3$Fe). As the grains of the Pt–Fe alloy obtained in this study were not studied by XRD, we do not know if they have the disordered face-

centered cubic structure of ferroan platinum or the primitive cubic structure of isoferroplatinum. The Pt–Fe alloy obtained in experiments could also represent a mixture of isoferroplatinum and tetraferroplatinum, unmixed from high-temperature ferroan platinum. A high base-metal content (PGE/BM < 3) and a high Ni/Fe value distinguish the synthetic Pt–Fe alloy from most of the natural analogues. However, some natural examples of Pt–Fe alloy with a high base-metal content (up to 35 at.%) and high Ni and Cu contents compare well to isoferroplatinum locally known from placers (Weiser & Bachman 1999).

(4) The first platinum sulfide, the synthetic analogue of natural cooperite (PtS), appears in a Cu-rich bulk composition (0.67 < Fe/Cu < 1) in association with Ni-rich Mss, Hz–Iss and Bn$_{ss}$ (Fig. 6e). As in some examples of the natural analogue, the synthetic cooperite is sulfur-deficient.

(5) The phase Cu(Pt,Ni,Fe)$_2$S$_4$ is present in sulfide associations with the highest bulk Cu-content (Fe/Cu > 0.6). Cu-rich Bn$_{ss}$ and Hz–Iss prevail in these assemblages, with extremely Ni-rich Mss (Fig. 6f). The corresponding natural analogue, malanite Cu(Pt,Rh,Ir)$_2$S$_4$, occurs in some platinum-bearing mafic–ultramafic complexes (Garuti *et al.* 1995, Barkov *et al.* 1997) and as inclusions in nuggets of Pt–Fe alloy (Cabri *et al.* 1996).

Palladium

In contrast to platinum, palladium is distributed mainly among the sulfide solid-solutions, with the quaternary solid-solution being its principal collector (Table 4). Only in the most Fe-rich part of the Me_9S_8 section does γ(Fe,Ni,Pd) alloy (up to 18.1 at.% Pd) occur, and the partitioning of Pd into the base-metal sulfide solid-solutions is very limited (Fig. 7a). A Pd(Cu,Fe) alloy is formed in Fe-rich bulk compositions lying along the Fe$_9$S$_8$–Cu$_9$S$_8$ join.

The Pd content of Hz–Iss ranges from 0.1 up to 1.5 at.% and increases as Ni and Cu abundances increase in Hz–Iss (Fig. 8a). The lowest Pd content occurs in the Fe-rich Hz–Iss, and the highest is found in the Ni-rich Hz–Iss. The Pd content was measured with the use of a defocused electron beam on the quenched Hz–Iss aggregates. The morphology of the Pd-bearing phases exsolved from the Hz–Iss matrix indicates that Pd entered into Hz–Iss structure at 760°C. Exsolved Pd-bearing phases include pentlandite (up to 1 at.% Pd), lamellar complex (Pd,Cu,Fe,Ni) sulfide (Fig. 7c, Table 4) and a Pd(Cu,Fe) alloy that occurs along boundaries of the original grains of Hz–Iss (Fig. 7b).

In addition to Hz–Iss, Pd also partitions into Mss. Its homogeneous distribution was confirmed by electron-microprobe analyses across profiles with a step interval of 3 μm. In Fe-rich Mss formed in the Fe-rich part of the Me_9S_8 section, Pd cannot be detected. In Ni-rich Mss from the central part of the Me_9S_8 section, Pd content may reach 0.1 at.%. Up to 0.9–1.1 at.% of Pd was fixed

in Ni- and S-rich Mss from the assemblages richest in Cu, where an equal distribution of Pd between Mss and Hz–Iss is observed (Fig. 8b).

Palladium was not found in bornite solid-solution, but lamellar exsolution-induced blebs of Pd-rich phases in a Bn$_{ss}$ matrix indicate its capacity to contain some Pd at elevated temperatures.

Platinum and palladium

Experiments conducted with trace amounts of Pt and Pd confirm the tendency of platinum to form its own phases. These phases may contain considerable amounts of palladium: up to 12.8 at.% in γ(Fe,Ni,Pt) alloy, 2.2 at.% in PtFe, 2.4 at.% in Pt–Fe alloys richer in Pt, and up to 4.8 at.% in PtS (Table 5). A very limited quantity of Pd (less than 0.3 at.%) was found at 760°C in synthetic malanite, as is found in natural analogues.

Rhodium

The physicochemical behavior of rhodium is remarkable, as it can either enter sulfide solid-solutions or form Rh minerals at very low or very high sulfur fugacity (Table 6). As in the case of Pd, secondary Rh-bearing phases may form by exsolution from an early high-temperature sulfide solid-solution.

In the starting composition richest in Fe, a γ(Fe,Ni, Rh) alloy with up to 27.1 at.% of Rh is stable (Fig. 7d). A Rh–Fe alloy with a composition close to that of ferrorhodium (FeRh) occurs in the Fe-rich part of the section (Fe/Cu = 7) in association with Fe-rich Mss and Hz–Iss. Ferrorhodium is rare in natural ore deposits; it was observed in the alloy-bearing type of platiniferous

Fɪɢ. 7. Back-scattered electron images. (a) Primary γ(Fe,Ni,Pd) alloy in association with Mss and quaternary solid-solution (decomposed light grey phase) (Pd-containing sample 7 after quenching from 760°C). (b) The quench-induced exsolution of phase Pd(Cu,Fe) along the boundaries between large grains of Hz–Iss (decomposed light grey phase) and Mss (Pd-containing sample 20 after quenching from 760°C). (c) Quench-induced exsolution lamellae of Pd-phase from the matrix of intermediate solid-solution stable in the Fe$_9$S$_8$–Cu$_9$S$_8$ join of the Me_9S_8 section (Pd-containing sample 28 after quenching from 760°C). Upper part of the figure is five times larger than of the lower one. (d) Primary γ(Fe,Ni,Rh) alloy coexisting with Mss and Hz$_{ss}$ (interstitial decomposed phase) (Rh-containing sample 1 after quenching from 760°C). (e) Enlarged view of the grain of the γ(Fe,Ni,Rh) alloy from the Figure 7d, with the γ(Fe,Ni) alloy exsolving from heazlewoodite solid-solution during the quench and forming a rim around the grains of primary Rh-bearing γ(Fe,Ni) alloy (same sample as in Figure 7d). (f) Skeletal crystals of the (Rh,Ni)S$_2$ phase stable in the Cu-rich association with Bn$_{ss}$ (light grey phase with exsolution lamellae of Iss) (Rh-containing sample 32 after quenching from 760°C).
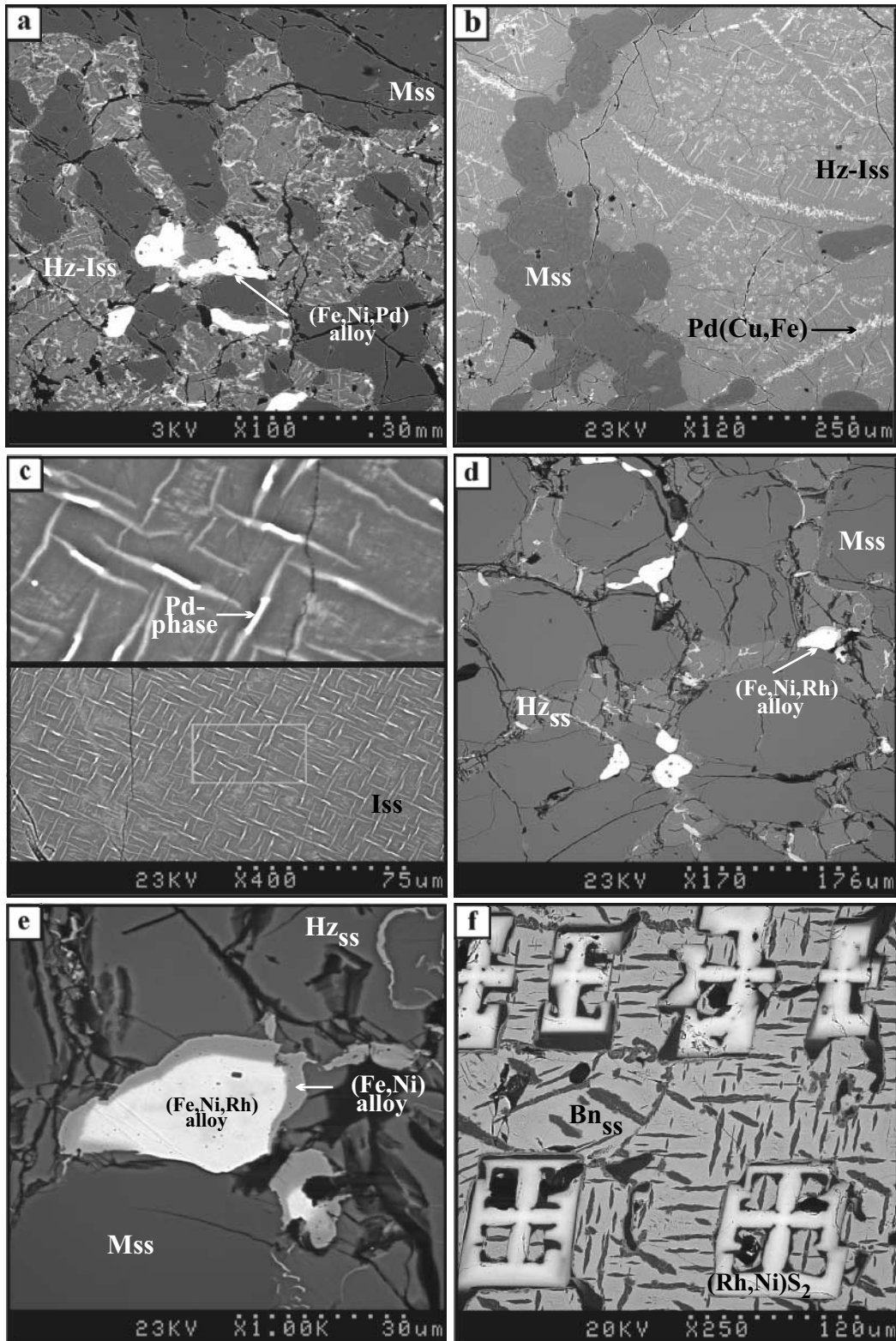
chromitites (Ohnenstetter *et al.* 1999). In our experiments, secondary γ(Fe,Ni) may rim the primary Fe–Ni–Rh alloy (Fig. 7e). The secondary γ(Fe,Ni) alloy is much lower in Rh than the primary one that precipitated from
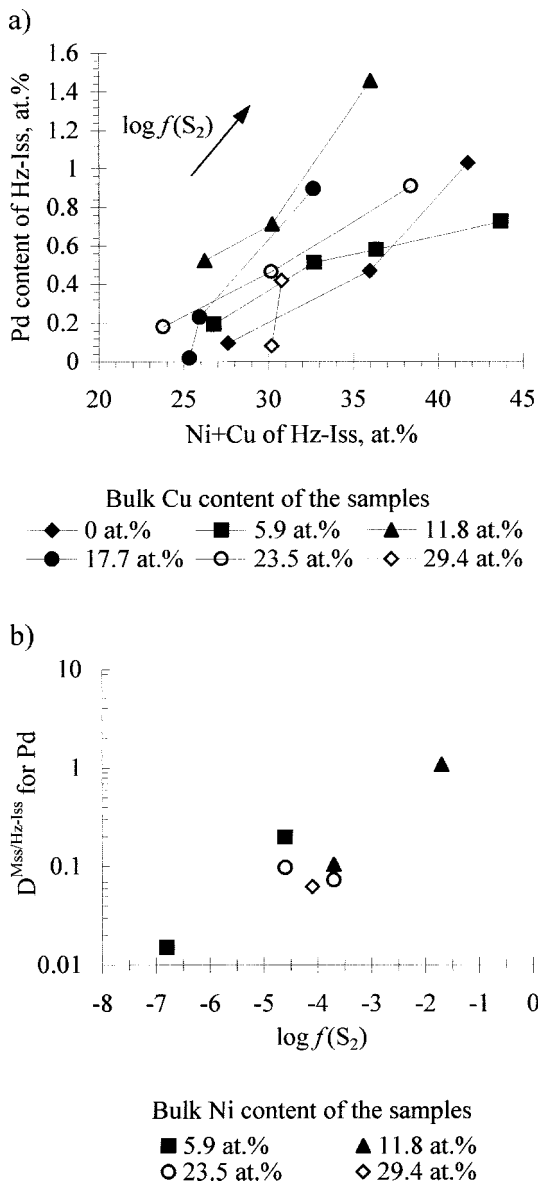
a)

b)

FIG. 8. (a) Correlation between Pd and Ni + Cu contents of the quaternary solid-solution stable in Me_9S_8 section at 760°C. The samples are grouped according to their starting concentrations of copper; the arrow shows the trend of increasing fugacity of sulfur. (b) Dependence of Pd partition coefficient between monosulfide and quaternary solid-solutions on sulfur fugacity. Note the logarithmic scale for $D^{Mss/Hz–Iss}$ values.

the sulfide liquid (Table 6). This difference is probably due to the very limited content of Rh in Hz_{ss} formed from Fe-rich bulk compositions. In Cu-rich runs, rhodium sulfides were observed. A phase similar to natural cuprorhodsite ($CuRh_2S_4$) appears in association with Cu-rich Iss, which occurs in the Ni-free side of the section. In the most Cu-rich assemblages, a rather unusual phase with a composition near $(Rh,Ni)S_2$ is stable, together with vaesite and Bn_{ss} (Fig. 7f).

In most of the section investigated (0.3 ≤ Fe/Cu ≤ 6), rhodium is distributed between Mss and Hz–Iss, but Hz–Iss is commonly poorer in Rh than Mss. No Rh was detected in Bn_{ss}. The Rh content of Mss varies from 0.59 up to 2.6 at.%, and there is a general tendency for Rh to increase with S content in Mss. Pyrrhotite solid-solution (Po_{ss}), stable on the Ni-free side of the Me_9S_8 section, contains an important quantity of rhodium, attaining 0.93 at.%. The Rh content of Cu-rich Hz–Iss is usually below the detection limit of electron-microprobe analysis, whereas that of Ni-rich Hz–Iss lies between 0.15 and 0.24 at.%, with a corresponding partition-coefficient of Rh between Mss and Hz–Iss ranging between 3 and 5.

The quench products from Hz–Iss were analyzed using a focused beam (2–3 μm, Table 6). Rhodium partitions in favor of pentlandite during cooling (up to 0.7 at.%), as opposed to Hz (Rh only in trace amounts), both of which formed as a result of breakdown of Ni-rich Hz–Iss. Pentlandite formed at the boundary between Mss and Hz–Iss during quenching below 760°C hosts significant amounts of Rh (up to 0.7 at.%).

Effect of bulk composition on f(S₂)

The position of isobars of sulfur fugacity projected onto the Me_9S_8 section is only approximate, as it is controlled by the direction of tie-lines connecting the coexisting phases located on each side of the Me_9S_8 plane. Despite this, $f(S_2)$ clearly varies with the base-metal proportions of the starting bulk-composition (Fig. 2a). Thus, $f(S_2)$ was found to increase significantly from log $f(S_2) = -10.5$ to values greater than zero where bulk Ni/Fe and Cu/Fe values increase in the system. Such large variation of $f(S_2)$ occurs despite the fact that the initial metal:S ratio and temperature were kept constant. In Fe-rich (Ni/Fe < 1; Cu < 12 at.%) samples, $f(S_2)$ increases from log $f(S_2) = -10.5$ to log $f(S_2) = -4.3$ with both bulk Ni- and Cu-contents (Fig. 9a); in Ni-rich (Ni/Fe > 1) samples or Cu-rich (Cu > 12 at.%) samples, the influence of Cu content is predominant over that of Ni, and $f(S_2)$ increases significantly from log $f(S_2) = -4.6$ to log $f(S_2) = -1.1$ as bulk Cu content increases in the samples (Fig. 9b). At these high levels of sulfur fugacity, S-rich phases like vaesite (NiS_2) and high-sulfur monosulfide solid-solution (>52 at.% S) appear in the BMS association. The extremely high $f(S_2)$ [log $f(S_2) \geq 0$] in the samples richest in Cu (Cu ≥ 29.4 at.%) is controlled by the presence of a sulfur liquid.

The phase assemblage and the mineral composition obtained from the experiments can be expressed as a function of $f(S_2)$, as shown in Table 7. To summarize, Fe-Mss to Ni-Mss, Hz–Iss, and Fe–Ni–PGE alloys (equivalent to natural Pt–Fe alloy and Rh–Fe alloy) are the stable forms under low-$f(S_2)$ conditions ($-10.5 < \log f(S_2) < -3.7$); Ni-Mss, Cu-rich Hz–Iss, Bn_{ss}, together with PGE sulfides (equivalent to natural cooperite, malanite, cuprorhodsite) characterize phase assemblages under high $f(S_2)$ [$\log f(S_2) > -3.7$]. Even without a determination of sulfur fugacity, the presence of PGE sulfides and S-rich Mss or vaesite (NiS_2) in association with Bn_{ss} is a good indication that even in a low-sulfur system, high $f(S_2)$ can be reached, in particular in Cu-rich associations.

Effects of f(S₂) on partition coefficients of Ni and PGE

Partition coefficients of Ni between monosulfide and quaternary solid-solutions ($D^{Mss/Hz–Iss}$ for Ni) increase strongly from 0.1 to 10.5 with increasing $f(S_2)$ and with the bulk Cu + Ni content of the samples (Fig. 10). A reversal in the trend of tie-lines connecting Mss and Hz–Iss is noted as Cu increases in the bulk rock (Fig. 5). For the Fe-rich compositions (Ni < 12–18 at.%; Cu < 12 at.%), Ni partitions in favor of Hz–Iss ($D^{Mss/Hz–Iss}$ for Ni < 1), and the tie-lines are pointing toward the nickel apex. For the compositions poorer in Fe, Ni preferentially accumulates in Mss ($D^{Mss/Hz–Iss}$ for Ni > 1), and tie-lines rotate counterclockwise toward the copper apex. In a set of experiments with the same initial bulk Cu-content, the resulting tie-lines progressively rotate toward the copper apex as the Ni:Fe ratio increases in the starting material. Ni in Mss increases with bulk Ni-content, and within a set of experiments at constant Ni-content, Ni in Mss increases with the initial Cu-content in the bulk samples, that is, with $f(S_2)$ (Fig. 11a). A positive correlation exists between Ni content of Mss and its S content, especially for Mss containing more than 18 at.% Ni (Fig. 11b). On the basis of structural considerations, the incorporation of Ni in the Mss structure is favored by the presence of vacancies, whose abundance increases with the S content of Mss (Li *et al.* 1996).

The reversal in the tie-line trend was observed in experiments at higher temperatures (1100°–850°C) between Mss and the sulfide liquid. For Fe-rich compositions, the liquid is characteristically enriched in Ni, and as Fe content and temperature decrease, the liquid is progressively enriched in Cu (Craig & Kullerud 1969, Fleet & Pan 1994, Li *et al.* 1996, Ebel & Naldrett 1996, 1997, Peregoedova 1998). All these studies confirm that the Ni enrichment of the residual liquid after Mss fractionation occurs only under conditions of low fugacity of sulfur in S-undersaturated and Fe-rich starting compositions. This finding emphasizes the fact that temperature is not the only important parameter to control the partition of Ni between Mss and the coexisting liquid or sulfide solid-solutions. The fugacity of sulfur, closely

related to the starting composition, remains the second major parameter that controls the evolution of the phase assemblage upon cooling. Hence, a Ni-rich sulfide liquid leading to Ni-sulfide deposits can be derived from parental Fe-rich and Cu-poor liquid after extensive fractionation of Mss.

Similarly to Ni, the partition coefficient (Mss/Hz–Iss) of Pd (Fig. 8b) and, to a lesser extent, Rh, increases
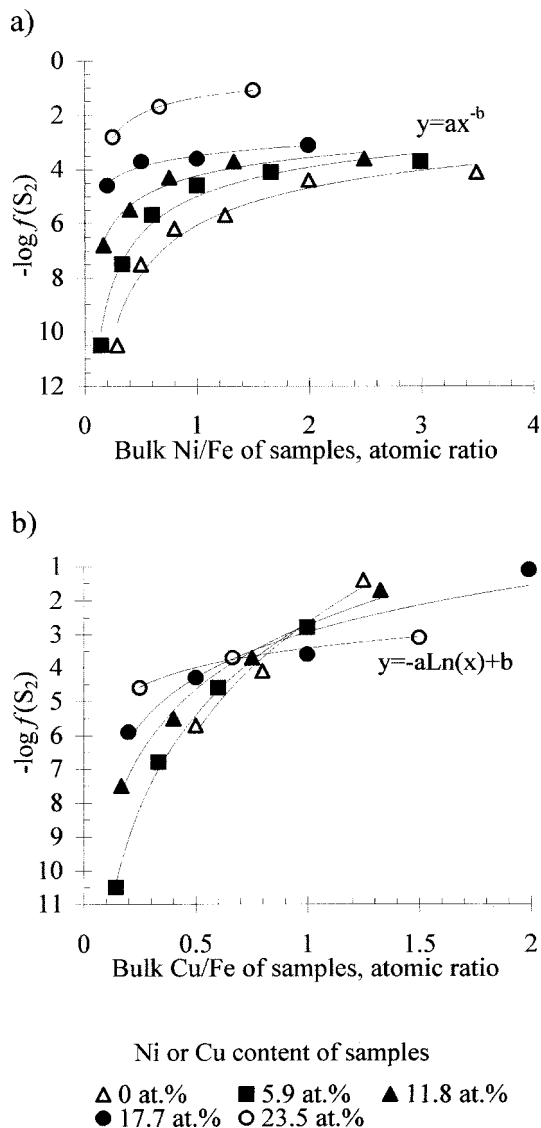
FIG. 9. Dependence of sulfur fugacity in the Me_9S_8 section at 760°C on (a) starting Ni:Fe ratio of the samples grouped according to the bulk Cu content, and (b) starting Cu:Fe ratio of the samples arranged according to the bulk Ni content.

with $f(S_2)$. This behavior is comparable to that observed in experiments performed at higher temperatures (1100°–850°C), which show the strong increase of the partition coefficients for PGE between Mss and liquid with the bulk S content (Li *et al.* 1996). However, a discrepancy is shown by Rh in experiments under S-undersaturated conditions performed either at high or low temperatures. At high temperatures (1000°C), Rh behaves incompatibly [$D^{Mss/L}$ for Rh = 0.37], the Rh content being eight times higher than the Pd content in Mss. In the present study, Rh behaves compatibly, as it preferentially partitions into Mss (0.59–2.6 at.%), in contrast to Pd (<0.1 at.%). These discrepancies concerning the behavior of Rh probably reflect the role of temperature on Rh partitioning between Mss and liquid.

DISCUSSION

Phase relations in the system Fe–Ni–Cu–S

One important result of the present study bears on the existence of a high-temperature Hz–Iss phase that coexists with Mss in most of the Me_9S_8 section. The composition of the Hz–Iss phase, covering a complete range between heazlewoodite (Ni,Fe)$_{3\pm x}$S$_2$ and intermediate Cu$_{1\pm x}$Fe$_{1\pm y}$S$_2$ solid-solutions, changes according to the initial proportion of the base metals (BM). The occurrence of Hz–Iss is reminiscent of the discovery of an unknown phase in S-rich compositions of the Fe–Ni–Cu–S system by Fleet & Pan (1994). During their investigation of the Fe-rich portion of the monosulfide plane (~52.5 and 50.0 at.% S, 800°–1050°C, and low pressure), Fleet & Pan (1994) reported a large field of a new ternary (Fe,Cu,Ni)S solid-solution (xss) intermediate between Iss and Mss, occurring at and below 850°C. The ternary solid-solution was found to have a stoichiometry close to that of cubanite (CuFe$_2$S$_3$). The lower metal:S ratio of "xss" compared to that of Hz–Iss could reflect the metal-rich composition of the starting assemblages in the present study.

No evidence of primary crystallization of pentlandite from sulfide liquid was found in the part of the system Fe–Ni–Cu–S investigated in the present experiments. Pentlandite only appears when monosulfide reacts with the quaternary solid-solution during quenching. In Cu-containing sulfide associations, pentlandite appears at subsolidus temperatures lower than 760°C and may incorporate the light PGE exsolved from their high-temperature collectors (Mss, Hz–Iss or Bn$_{ss}$).

As pentlandite is a common phase in PGE-bearing sulfide deposits, natural Cu–Ni sulfide ores represent the final result of various low-temperature reactions accompanying subsolidus re-equilibration. Hence, only rarely is the evidence preserved for the presence of high-temperature sulfide solid-solutions from the early stage of ore formation. Recently, high-temperature cubanite, chalcopyrite and Ni-rich monosulfide solid-solutions have been described from the zone of wedging of vertical sulfide veins in the Norilsk–1 deposit (Distler *et al.* 1996). Pasteris (1984) found assemblages of pyrrhotite with cubanite to be stable among the Cu–Fe–Ni sulfides of the Duluth Complex, both containing pentlandite inclusions. Partial replacement of Fe sulfides by massive cubanite was proposed as a possible interpretation of this association. According to our experimental data, which reveal a high solubility of Ni in the intermediate solid-solution, this association may also be explained by the breakdown of Ni-bearing Fe-rich Iss (*i.e.,* the quaternary solid-solution Hz–Iss), and of Mss upon cooling, whereby both Mss and Hz–Iss solid-solutions exsolve surplus Ni as minute grains of pentlandite, which are very typical in experimental samples.

TABLE 7.   PGE-BEARING ALLOYS, SULFIDES, AND BASE-METAL SULFIDE ASSOCIATIONS
STABLE AT 760°C IN THE SECTION Me$_9$S$_8$ OF THE SYSTEM Fe-Ni-Cu-S.

log $f(S_2)$	BMS association	PGE-bearing phases		
		Pt	Pd	Rh
-10.5	Fe-Mss, Hz-Iss with Fe>Ni>Cu	γ(Fe,Ni,Pt)	γ(Fe,Ni,Pd) or Pd(Cu,Fe)	γ(Fe,Ni,Rh) or FeRh
-7.5 ÷ -5.5	Fe-Mss, from Hz-Iss with Fe>Ni>Cu to Ni-rich Hz-Iss	Pt-Fe alloys Pt/Fe ≈ 1	up to 2.2 at.% Pd in Pt-Fe alloy	0.6-0.9 at.% Rh in Mss up to 0.2 at.% Rh in Hz-Iss
-5.7 ÷ -3.7	from Fe-Mss to Ni-Mss, from Hz-Iss with Fe≈Cu>>Ni to Ni-rich Hz-Iss	Pt-Fe alloys 1.5<Pt/Fe<2.5	up to 1.5 at.% Pd in Hz-Iss up to 0.1 at.% Pd in Mss up to 2.4 at.% Pd in Pt-Fe alloy	up to 0.9 at.% Rh in Mss
-3.6 ÷ -1.7	Ni-Mss, Bn$_{ss}$, Hz-Iss(Cu>Fe>>Ni)	PtS	up to 0.9 at.% Pd in Mss and Hz-Iss up to 4.8 at.% Pd in PtS	up to 2.6 at.% Rh in Ni-Mss
>-1.4	Ni-Mss, Bn$_{ss}$, Hz-Iss(Cu>Fe>>Ni)	CuPt$_2$S$_4$	2 at.% Pd in Ni-Mss 0.1 at.% Pd in Hz-Iss 0.1 at.% Pd in CuPt$_2$S$_4$	CuRh$_2$S$_4$
>0	Vs, Bn$_{ss}$	*no data*	0.2 at.% Pd in Bn$_{ss}$ 0.1 at.% Pd in Vs	(Rh,Ni)S$_2$

Another interesting point in terms of phase relations in the Me_9S_8 section is the presence of a high-sulfur phase, vaesite, NiS_2, in spite of S-poor starting composition (Figs. 1, 2). The appearance of vaesite for Cu-rich starting composition is due to the existence of the three-phase association $Vs + Bn_{ss} + S_L$, known to be stable in the Fe–Ni–Cu–S system at 760°C (present study) and at 650°C and 550°C (Craig & Kullerud 1969). The Me_9S_8 section (47 at.% S) presently investi-gated intersects the three-phase association and the tie-lines connecting vaesite and S-poor phase, bornite solid-solution (39.9 ≤ S at.% ≤ 43.5). According to Craig & Kullerud (1969), these tie-lines appear in the system Fe–Ni–Cu–S at 816°C when "the sulfide-rich liquid field is reduced sufficiently in size so that Vs and Bn_{ss} can co-exist".

a)

a)

b)

b)

Bulk Ni content of the samples

■ 5.9 at.%   ▲ 11.8 at.%   ● 17.7 at.%
○ 23.5 at.% ◇ 29.4 at.%   □ 35.3 at.%
△ 41.2 at.%
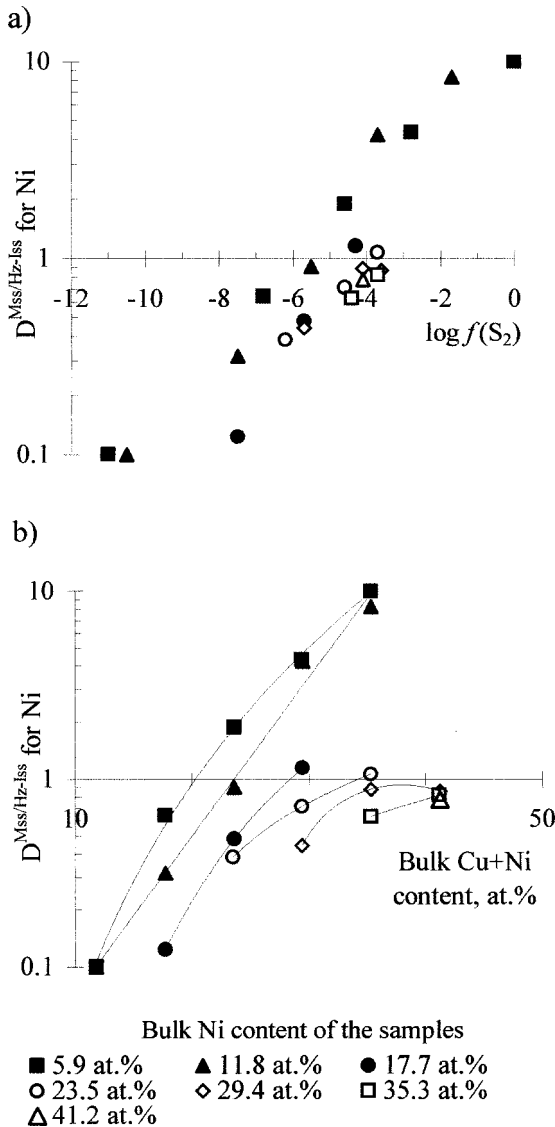
FIG. 10.   Dependence of Ni partition coefficient between monosulfide and quaternary solid-solutions on (a) sulfur fugacity, and (b) bulk Cu + Ni content of the samples. Note the logarithmic scale for $D^{Mss/Hz–Iss}$.

Bulk Ni content of the samples

-■- 5.9 at.%   -▲- 11.8 at.%   -●- 17.7 at.%
-○- 23.5 at.% -◇- 29.4 at.%   -□- 35.3 at.%
-△- 41.2 at.%
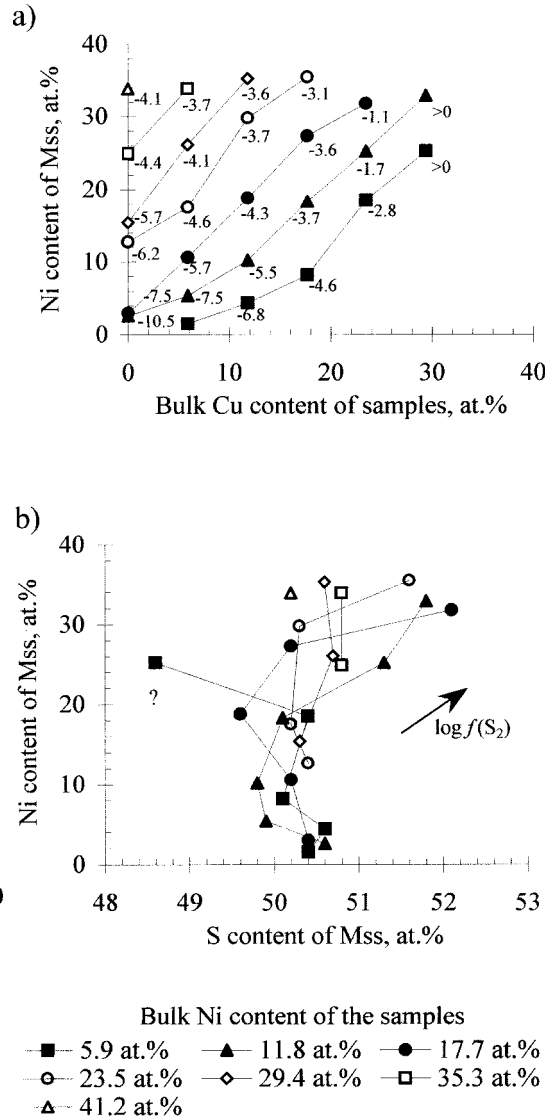
FIG. 11.   (a) Dependence of Ni content of monosulfide solid-solution stable at 760°C on the bulk Cu content and sulfur fugacity (samples are grouped according to bulk Ni contents). Measured sulfur fugacity is indicated near each sample in terms of log $f(S_2)$. (b) Correlation between Ni and S content of the monosulfide solid-solution in the range of samples with constant bulk Ni content. The arrow indicates the trend of increasing fugacity of sulfur.

Partitioning of PGE in sulfide associations:
a comparison with previous experimental studies

The contrasting behavior of Pt and Pd is emphasized by the present experiments, with Pt forming its own phases and Pd preferentially partitioning into Hz–Iss. Our findings complement the preceding investigation in the system Fe–Ni–S at 1000°C (Fleet & Stone 1991) and in the Fe–O–S system (1000°–1375°C, 4.5 to 11 GPa) under low $f(S_2)$ with minor amounts of PGE added (Fleet *et al.* 1991). All the experiments conducted under S-poor conditions emphasize the compatible character of Pt over a large range of temperature (1100° to 760°C). In a S-poor system, Pt–Fe alloy together with Mss are early-formed phases, which may crystallize before the appearance of Hz–Iss by a peritectic reaction. Such a reaction between Mss and a sulfide liquid may occur at 908°–795°C according to our preliminary experiments, done in the same system but at higher temperatures, or at 850°C and below in a S-saturated system (Fleet & Pan 1994). At high temperatures (about 1000°C), in S-undersaturated experiments, Mss is the only stable sulfide solid-solution (Kullerud *et al.* 1969) and is associated with Pt–Fe alloys (Fleet & Stone 1991, Fleet *et al.* 1991). In contrast, under S-saturated conditions, both Pt and Pd are partitioned into a sulfide liquid (Fleet *et al.* 1993), and Os, Ir, Ru and Rh enter Mss. Pyrrhotite may dissolve 44 wt.% Rh, 11% Pd, 3.6% Ru and 1.2% Pt under high fugacity of sulfur at temperatures of 900°C (Makovicky *et al.* 1986). All these experiments indicate a higher solubility of Pd and, in a more general way, of other light PGE in Mss, when compared to Pt. Ballhaus & Ulmer (1995) showed that the maximum solubilities of Pt and Pd in $Fe_{1-x}S$ at the pyrrhotite – sulfide liquid equilibrium at 850°C are about 1.1 and 6.5 wt.%, respectively.

The present experiments emphasize the dual behavior of Rh, which either enters Mss or forms its own mineral phases under very high or very low sulfur fugacities. Compared to Pd, Rh enters preferentially into Mss, as shown by experiments performed at 1100°C under S-saturated conditions (Ebel & Campbell 1998). Their results also indicate that as the $f(S_2)$ decreases, the partition coefficients for Rh and Pd between Mss and liquid also decrease, and Rh can preferentially partition into sulfide liquid, like Pd. However, our experiments show that the behavior of Rh could change under S-undersaturated conditions, with the appearance of Rh–Fe alloys at low fugacity of sulfur.

APPLICATIONS TO Pt AND Pd DEPOSITS

The application of experimental results to natural deposits is generally hampered by a poor knowledge of the initial composition of the sulfide liquid parental to the deposits. It is generally accepted that the metal:S ratio of sulfide liquid does not commonly exceed the compositional field of pyrrhotite (Naldrett 1989). How-

ever, in this range of composition, a large variation in partition coefficients of base metals and PGE between the early Mss and the sulfide liquid has been reported (Li *et al.* 1996), which should result in contrasting distribution of the PGE within sulfide ores. Massive sulfide ores (*e.g.*, at Sudbury and Noril'sk) are generally considered to derive from a S-saturated system (50–52.5 at.% S). This view agrees with the fact that both Pt and Pd in such deposits are concentrated in the residual Cu-rich sulfide liquid (Li *et al.* 1992), and is also supported by experimental results performed with a S-saturated melt or under a high fugacity of sulfur (Naldrett *et al.* 1997, Li *et al.* 1996).

The present experiments were conducted in a S-poor system, which emphasizes the contrasting behavior of Pt and Pd. If a sulfide melt with high metal:S ratio (*Me/S* > 1) could occur in natural conditions, how would one recognize its former presence? A high metal:S ratio, ranging between 1 and 1.087, is recorded in some sulfide globules found in basaltic lavas from mid-oceanic-ridge settings (Czamanske & Moore 1977). Magmatic sulfide liquid coexisting with silicate magma at the time of eruption thus could have a low bulk-S content, at least lower than that assumed for sulfide liquids, parental to massive sulfide deposits.

According to experiments done under conditions of extremely low sulfur fugacity, a low-S (47 at.%) but Fe-rich sulfide melt should involve fractionation of PGE as a result of separation of a metal-rich solids from the sulfide liquid, with Pt partitioning into alloy and Pd into the sulfide liquid. In the following section, PGE deposits hosting abundant Pt–Fe alloys will be preferentially considered in applying our experimental results. The preponderance of Pt–Fe alloys among other PGE mineral species generally skewed the Pt:Pd ratio toward high values. This leads to the recognition of an alloy type of platiniferous mineralization, which can be found in diverse settings ranging from mantle rocks to layered complexes, as in ophiolite complexes and in the Merensky Reef (Ohnenstetter 1996). In all of these PGE deposits, the proportion of base-metal sulfides is low, below 2%, and may even be nearly absent, as in Pt deposits located in the crustal sequence of some ophiolites.

PGE anomalies within mantle peridotites

Base-metal sulfides are commonly present in trace amounts within mantle peridotites, in which they are locally associated with PGE anomalies (Lorand *et al.* 1993). Whether the sulfur component is of residual origin, having survived the partial melting event, or related to deposition of immiscible droplets during percolation of a S-saturated silicate melt, is still debated. However, there is increasing evidence that sulfide-rich occurrences, heterogeneously distributed within the mantle rocks, directly depend on whether the residual peridotites contain trapped silicate melts.

Among the first PGM described in mantle rocks are two Pt–Fe alloy grains (Pt_3Fe) found in peridotite nodules in kimberlites (Stone & Fleet 1990). The composition of the alloys approaches that of a Pd-rich isoferroplatinum (5.6 and 3.9 at.% Pd in each grain). The grains occur in a polymineralic subspherical sulfide bleb located in or adjacent to fractures within olivine megacrysts (Fo_{90}). One bleb contains lamellar intergrowths of pyrrhotite and pentlandite in its center; these are surrounded by single-phase pentlandite and a margin of chalcopyrite associated with the Pt–Fe alloy. In both blebs, the Pt–Fe alloy grains occur along the contact between chalcopyrite at the bleb margin and the surrounding olivine. One may consider that the Pt–Fe alloy, associated with chalcopyrite, is either a late-stage product from residual Cu-rich sulfide liquid upon cooling, or an early-stage precipitate that crystallized from the margin of the bleb toward the center of the sulfide liquid droplet, in equilibrium with the high-temperature Mss. The observation of a lath of Pt–Fe alloy partly included in an olivine crystal hosting a sulfide bleb agrees with the latter hypothesis. According to this texture, the late-stage residual Cu-rich liquid was forced to crystallize at the margin of the droplet, and consequently partly enclosed the early-formed Pt–Fe alloy. The zonal texture displayed by pyrrhotite and pentlandite is compatible with the present experiments, which predict early crystallization of Mss followed by Hz–Iss formed during reaction of Mss with the trapped residual sulfide liquid during cooling.

In the Jurassic ophiolites of Corsica, minute crystals of Pt–Fe alloys together with sparse grains of base-metal sulfides host the Pt and Pd anomalies locally found within pyroxene-rich lherzolite, harzburgite and dunite (Ohnenstetter 1992). Pt and Pd contents reach up to 130 ppb and 20 ppb, respectively. Pentlandite is a prevalent phase among BMS, consisting of pyrrhotite, millerite and rare bornite, covellite and chalcopyrite. Most of the BMS and PGM occur in interstices between olivine and pyroxene crystals. On the basis of this textural arrangement, Ohnenstetter (1992) suggested that the deposition of high-temperature Fe- and Ni-rich sulfides occurred in narrow magmatic pathways (<10 mm) during an upward migration of silicate magmas through mantle rocks at the mid-oceanic ridge environment. The main carriers of PGE and gold are alloys (85%) and tellurides (10%). The stoichiometry of the small grains of Pt-Fe alloys (<1 μm) is close to that of tetraferroplatinum. Grains occur inside or at the rim of pentlandite, locally with awaruite. Tellurides occur preferentially with Cu sulfides. We cannot exclude the possibility that all the BMS and PGM, notably the Pt–Fe alloys, are secondary phases formed during serpentinization. However, considering the present experiments, we can suggest that the Pt–Fe alloys represent early magmatic phases, formed in equilibrium with a high-temperature sulfide solid-solution. In this case, the small-scale zonal distribution of BMS and PGM with a central part of alloys

and Fe–Ni sulfides, surrounded by rare disseminated Cu-rich sulfides and Pd tellurides, could result from an *in situ* crystal fractionation of the sulfide liquid trapped between silicate minerals. In addition, the predominance of tetraferroplatinum in this oceanic-lithosphere-type of mantle segment would indicate derivation under a lower fugacity of sulfur than that prevailing during deposition of isoferroplatinum and Pd-bearing pyrrhotite (0.61 wt.% Pd) in the mantle under Fayette County, Pennsylvania (Stone & Fleet 1990).

The presence of BMS in mantle peridotites from the Upper Eocene ophiolitic nappe in New Caledonia was recognized a long time ago (see a review in Augé *et al.* 1999), and these constituted a source for the supergene Ni deposits. The proportions of nickel-bearing sulfides, Cu-bearing sulfides and iron-bearing sulfides are estimated as follows: Ni:Cu:Fe = 95:4:1. Several mineralogical features indicate the former presence of Cu-rich high-temperature solid-solutions: intergrowths between pentlandite and chalcocite, and bornite with exsolution of chalcopyrite (Guillon & Lawrence 1973). Two major contrasting occurrences were described in detail, and BMS together with alloys were analyzed to study the PGE distribution in bulk-rock and mineral concentrates (Augé *et al.* 1999). In the Massif du Sud, at Yaté, the mineral assemblage comprises awaruite and heazlewoodite in variable proportions; they are usually found between silicate grains in close association with spinel. Awaruite forms a symplectite with spinel or occurs as small grains coexisting with spinel, within silicates. Pentlandite hosting trace amounts of PGE (1–10 ppm Pt) is clearly a secondary phase forming a halo around heazlewoodite. In Néou Mindiou, located in the Intermediate Massifs, northwest of Massif du Sud, pentlandite is the predominant BMS over heazlewoodite. In the two occurrences described, rods of millerite and native Cu in heazlewoodite may indicate the existence of a previous high-temperature sulfide solid-solution containing Fe, Ni and Cu. Likewise, rods of native copper within or around awaruite may suggest that a high-temperature Cu-rich Fe–Ni alloy coexisted with this high-temperature sulfide.

The maximum bulk PGE content in peridotites is low (43.5 ppb at Yaté, and 191 ppb at Néou Mindiou, respectively). PGE anomalies were located in the sulfide and alloy concentrates, with maximum values of 9,718 ppb Pt and 11,494 ppb Pd. The Pt:Pd ratio of the concentrates is a discriminant, and generally contrasts with bulk-rock samples, in which Pt/Pd is below unity (0.2–0.7). At Yaté, the high Pt/Pd value (about 2) measured in some concentrates may be correlated with the high proportion of alloys. According to SIMS analyses, Pt is mostly located in awaruite, which shows a range from 0.002 to 0.121 wt.% Pt, whereas no Pt was detected in heazlewoodite. It is remarkable that the highest Pt/Pd value (2.5) was found in a concentrate devoid of BMS, and the lowest one (0.6) comes from a concentrate with the highest proportion of heazlewoodite. A similar cor-

relation can be established at Néou Mindiou, suggesting that primary distribution of the PGE is preserved at a small scale within samples of mantle rock, as proposed by Augé *et al.* (1999). The process of PGE fractionation deduced from the phase assemblage and the non-chondritic ratio of the concentrates would involve an early precipitation of Pt within alloys and a late-stage deposition of Pd in high-temperature sulfide solid-solution. The efficient separation of alloys from the residual sulfide liquid would explain the large variation of the Pt/Pd values observed between the concentrates and the bulk rocks.

Other PGM found in mantle peridotites are diverse and occur within BMS or as satellite grains surrounding BMS. Arsenides, tellurides and various alloys have been described from the Lizard and Troodos lherzolites, commonly in association with Cu-rich sulfides (Hutchinson *et al.* 1999). This assemblage is similar to that commonly found in Cu-rich ores and contrasts with those described above, in which the abundances of Cu sulfides are low, and most of the PGE are contained in alloys.

On the basis of the present experiments, a preliminary comparison of PGM occurrences within mantle rocks suggests their derivation from magmatic sulfide liquids of variable composition, crystallizing under various fugacities of sulfur. Further discussion of the base-metal:S ratio and of the Ni/Cu value of sulfide melts that percolated through the mantle is beyond the scope of this paper. Suffice it to say that the Ni:Cu ratio of the sulfide liquid is controlled by that of the coexisting immiscible silicate liquid, the composition of which is directly buffered by mantle peridotites. Sulfide liquids with the highest Cu contents are expected to form from fertile peridotites having undergone moderate partial melting (*e.g.,* in Lizard), or in the subcontinental mantle peridotites, as sampled by kimberlites. Sulfide melts containing the lowest Cu contents are expected to segregate from silicate liquids derived from strongly depleted peridotites in island-arc to back-arc basin settings or from ophiolitic peridotites in such geotectonic environments. This proposal agrees with the distinct metallogenic potential of high-Ti and low-Ti basaltic magmas respectively, occurring in mid-oceanic ridge and island-arc settings (Hamlyn *et al.* 1985).

Application to the Bushveld Complex

The UG2 chromitite-rich layer and the overlying Merensky Reef, consisting of pegmatitic pyroxenites, are the two main PGE-mineralized layers in the Bushveld Complex. In both layers, the Pt:Pd ratio is high, about 2 (McLaren & De Villiers 1982) and cannot be explained by fractionation alone, suggesting that the PGE distribution between sulfide and silicate liquid, and between Mss and sulfide liquid, is approximately similar (Maier & Barnes 1999). The Merensky Reef contains less than 2% of base-metal sulfides, and the UG2

chromitite generally contains much less. Among the two reefs, the nature of PGM in association with BMS is extremely diverse, and predominant Pt phases may be either alloys, sulfides, arsenides, tellurides or intermetallic compounds, which are regionally distributed (Kinloch 1982).

Vermaak & Hendricks (1976) described a typical Merensky Reef assemblage with interstitial globules of polyphase sulfides between silicates. Sulfide aggregates contain a core of round to angular pyrrhotite included in pentlandite, itself rimmed by chalcopyrite. According to these authors, all mineralogical evidence suggests that the BMS blebs began to crystallize at the center; the crystallization of pyrrhotite is followed by that of pentlandite and chalcopyrite in that order. In the Rustenburg area, Pt–Fe alloys and sulfides of Pt and Pd are predominant over other mineral species (>60%). Pt–Fe alloys have a euhedral habit inside pyrrhotite and show no tendency to be enclosed in chalcopyrite, a fact compatible with an early deposition of alloys together with a high-temperature Mss. In addition, Pt–Fe alloys locally form delicate intergrowths of variable size with Fe sulfide. The latter texture is indicative of eutectoid-type crystallization, and constitutes irrefutable evidence of the contemporaneous crystallization of the Pt–Fe alloys and base-metal sulfides. Cooperite commonly occurs within pentlandite, which crystallized from a high-temperature Fe- and Ni-rich sulfide solid-solution. Cooperite may enclose the Pt–Fe alloys, or locally form a complex intergrowth with them. According to our experiments, this relationship illustrates a local increase in $f(S_2)$ after the early deposition of alloys and Mss. The scarcity of Pd minerals and the preferential concentration of Pd in pentlandite (Ballhaus & Sylvester 2000) reflect the incompatible behavior of Pd, which accumulates in the residual Cu-rich sulfide liquid. Interestingly, Kinloch (1982) noted that where the major PGM is Pt_3Fe (*e.g.,* in the Union section), the solid solution of PGE in pentlandite reaches higher values than in areas where Pt–Pd sulfides are the major PGM. In contrast, about 30 km west of Rustenburg, at Impala mines, nearly no Pt–Fe alloy is present, and most of the Pt and Pd minerals are moncheite and sulfides (cooperite, braggite). In addition, there is a remarkable tendency of these PGM to occur with chalcopyrite (Mostert *et al.* 1982). In UG2, sulfides or Pt–Fe alloys are generally predominant over the other mineral species. Sulfides consist of laurite, cooperite, braggite and vysotskite, together with complex solid-solutions of Pt–Ir–Rh–Cu sulfides and Pt–Pb–Cu sulfides (McLaren & De Villiers 1982). In the section exhibiting predominant alloys, the Pt–Fe alloys may occur as early-formed skeletal grains within BMS. Interestingly, an example of fractionation of the sulfide liquid is described from angular sulfide inclusions within the lower chromitite of the UG–2 layer in the western sector of the eastern Bushveld (von Gruenewaldt *et al.* 1990). The presence of bornite, the "talnakhite-type" of chalcopyrite and pentlandite with a

high Fe:Ni ratio indicates that chromite grains trapped a sulfide liquid of composition different from the bulk interstitial sulfides. The PGE–Ni- and Cu-rich sulfide liquid was trapped in chromite after significant fractionation of Mss close to 1190°C.

The close similarity between the assemblage of PGE minerals observed in the Merensky Reef and the UG2 layer, dominated by Pt–Fe alloys and sulfides, and that produced by the present experiments, provides good evidence for a common primary magmatic origin of BMS and PGM. An early-stage deposition of Pt is suggested where a Pt–Fe alloy is associated with Mss, and later-stage deposition where cooperite is associated with Fe- and Ni-rich sulfides. The deposition of Pt could have occurred even later where arsenides and tellurides are associated with Cu-rich sulfides. The change in the mineral species hosting Pt as well as the different timing of Pt deposition with respect to the associated BMS imply important variations in sulfur fugacity during the deposition of PGE in the mineralized layers, notably in the Merensky Reef.

The alloy type of PGE mineralization in ophiolites and Alaskan-type intrusions

The style and type of PGE mineralization in ophiolites are diverse, considering the host-rock lithology, the proportion of BMS, the dominant carrier and the distribution of the PGE. An alloy-bearing type of PGE mineralization was defined in some chromitites associated with dunites and pyroxenites located in the transition zone between mantle rocks and the cumulate sequence (Ohnenstetter 1996). This mineralization is characterized by the predominance of the Pt–Fe alloys and the scarcity of Pd minerals as well as of BMS, which skews the Pt:Pd ratio toward high values (up to 100). Alloy-bearing platiniferous chromitites occur in Thetford Mines, Quebec (Corrivaux & Laflamme 1990, Gauthier *et al.* 1990), Tropoja, Albania (Ohnenstetter *et al.* 1991, 1999), and in New Caledonia (Augé & Maurizot 1995, Augé *et al.* 1998). Such chromitites were also recognized in the dunitic core of zoned or Alaskan-type complexes, such as the Tulameen complex (Nixon *et al.* 1990) and the Condoto complex, northwestern Columbia (Tistl 1994). The mechanical erosion of zoned complexes is generally considered to be responsible for the formation of placer deposits, mainly consisting of Pt–Fe alloys.

Because of the predominance of Pt–Fe alloys, the alloy-bearing type of Pt mineralization may be a good candidate for natural analogues of experiments under extremely low-S conditions. However, direct application of the present experiments is prevented by the extremely low amount of BMS, a fact exhibited by both the Alaskan-type complexes (Nixon *et al.* 1990, Slansky *et al.* 1991) and the ophiolites (Augé & Maurizot 1995). In a more general way, Melcher *et al.* (1997) noticed that the "primary PGM" in ophiolites are only rarely associated with base-metal minerals. Because of the low amount of BMS, the origin of the Pt–Fe alloys is debated. Did they crystallize from a sulfide liquid, which preferentially collected PGE, or directly from a silicate magma (Nixon *et al.* 1990), in which PGE could be concentrated in clusters (Tredoux *et al.* 1995, Ballhaus & Sylvester 2000, Barnes & Maier 2002). Direct precipitation of the PGM from a silicate magma cannot be excluded, as spherical globules of silicate-glass inclusions, ranging from basic to felsic in composition, have been found in the Pt–Fe alloys (Johan *et al.* 1990, 1991, Augé & Legendre 1992, Gornostayev *et al.* 1999). Likewise, the existence of a sulfide liquid is convincingly depicted by the presence of subspherical polyphase sulfide blebs within Pt–Fe nuggets, which crystallized from a trapped sulfide melt (see below; Johan *et al.* 1990, Gornostayev *et al.* 1999, Tolstykh *et al.* 2000). Simultaneous entrapment of sulfide and silicate inclusions within the Pt–Fe alloys is deduced from the occurrence of coexisting blebs of sulfides with silicate glass inclusions (Johan *et al.* 1990). This finding indicates an incomplete separation of sulfide liquid from the silicate magma during the simultaneous crystallization of Pt–Fe alloys and the surrounding chromite. These relationships would suggest that a small amount of sulfide melt had segregated from the evolving S-saturated silicate magma, or that the sulfide melt was expelled from the site of chromite deposition during compaction. The latter process would have led to a major fractionation of Pd from Pt, as illustrated by the high Pt/Pd value observed in instances of alloy-type PGE mineralization.

In the alloy-bearing platiniferous chromitites, sulfide minerals consist predominantly of PGM. The main phases reported in the Tropoja deposit in Albania consist of 21% PGE sulfides and 73% alloys (Ohnenstetter *et al.* 1999). Other mineral species are sulfarsenides, arsenides and tellurides. Compounds of Pt with As, Te and Sb are not commonly reported. However, besides Pt, all the PGE could have locally formed arsenides or sulfarsenides. The presence of anduoite, $(Ru,Os)As_2$, instead of laurite within a chromite grain from Tropoja, Albania and Kapitanov, Ukraine, is interpreted as evidence of high activity of As in relation to very low $f(S_2)$ (Gornostayev *et al.* 2001) during magmatic deposition of chromite.

Sulfides of the iridium group of PGE (IPGE, Os + Ir + Ru; Barnes *et al.* 1985), notably laurite, typically the first sulfide to crystallize, but also bowieite and kashinite, are locally found as discrete inclusions within Pt–Fe alloys. Laurite may also occur in polyphase aggregates with the alloys. IPGE sulfides may be replaced by IPGE alloys, which coexist with isoferroplatinum, commonly showing high contents of IPGE in solid solution (Augé *et al.* 1998). The distribution of the IPGE alloys and sulfides indicates that the coexisting Pt–Fe alloys were formed under distinct conditions of $f(S_2)$. According to the experiments on stability limits of laurite and Ru–Os–Ir alloys as functions of temperature

and sulfur fugacity within the range recorded by basaltic magmas, Brenan & Andrews (2001) suggested that these phases could be primary magmatic solids, crystallizing together with spinel from a silicate magma that did not reach saturation to form an immiscible sulfide liquid. It is remarkable that the *in situ* alloy-bearing platiniferous chromitites generally have a high ratio of platinum-group PGE (PPGE) to IPGE, which indicates an episode of early removal of the IPGE, either from the sulfide melt or even earlier, from the silicate magma. This inference lends credence to the direct crystallization of early-formed Pt–Fe alloys with IPGE alloys or sulfides under sulfide-liquid-absent conditions.

Cooperite (PtS) is rare in ophiolites and Alaskan-type complexes, compared to the intrusions hosting PGE-mineralized sulfide reefs. In the former, cooperite is found as single discrete crystals in Pt–Fe alloy or in polyphase association with the thiospinel group of sulfides (malanite, cuprorhodsite, cuproiridsite), whose composition is of the $(Cu,Fe)(Pt,Ir,Rh)_2S_4$ type. The occurrence of cooperite and, more importantly, of the thiospinel group of sulfides confirms the fact that a locally high fugacity of sulfur is reached, even in a low-S deposit. Cooperite rimming Pt–Fe alloys is considered to be characteristic of the Uralian (Alaskan-type) massifs (Tolstykh *et al.* 2000). A distinct composition is exhibited by cooperite included in Pt–Fe nuggets and that rimming the nuggets, the former being richer in Pd. In the Pirogues River deposit, New Caledonia, proportions of cooperite and Pt–Fe alloy varying from one deposit to another within the Pt-enriched chromitite zone (Augé & Maurizot 1995) indicate that the sulfur fugacity hovered above that of the sulfuration curve of platinum.

In ophiolites, the more commonly reported BMS is heazlewoodite, which occurs between chromite grains. Corrivaux & Laflamme (1990) described heazlewoodite (1–200 μm in diameter) associated with Pt–Fe alloys within a serpentine matrix enclosing chromite. A similar setting is reported for a Pd-rich heazlewoodite (3.3 wt.% Pd) from the Great Serpentinite Belt, Australia (Yang & Seccombe 1993). This association is compatible with our experimental observations indicating the early crystallization of Pt minerals, in this case Pt–Fe alloys, followed by the crystallization of a Pd-rich high-temperature solid-solution, such as Hz–Iss. In the Tulameen complex, in British Columbia, pyrite is the more common sulfide, but heazlewoodite and millerite, together with pentlandite, violarite and bravoite, are reported as occurring between chromite grains and in small veins (Nixon *et al.* 1990). The bulk composition of this phase assemblage indicates the existence of a residual Ni- and Cu- rich melt (provided the initial metal contents and metal/S values were preserved), which could have crystallized under high $f(S_2)$. This conclusion is independently corroborated by the local occurrence of the thiospinel group of minerals.

In the alloy type of PGE mineralization, Pt–Fe alloys (generally euhedral and smaller than 30 μm) are the preponderant carriers of Pt. They are commonly included within chromite crystals. Large anhedral crystals of Pt–Fe alloy (up to 200 μm) may also occur as single grains or within polyphase aggregates between chromite or olivine grains. In dunite from the Alto Condoto Complex, Pt–Fe alloys and chromite form intergrowths interpreted as indicative of contemporaneous crystallization (Tistl 1994). A wide range of compositions is encountered, from an iron-rich alloy such as Pt-bearing awaruite to ferroan platinum. An awaruite grain with a high content of Pt (32.5–47.1 wt.% Pt) was described in the Thetford Mines ophiolites (Corrivaux & Laflamme 1990). Most of the Pt–Fe alloys approach the composition of isoferroplatinum (Pt_3Fe), tetraferroplatinum (PtFe) and tulameenite (Pt_2CuFe). However, there is strong departure from the ideal stoichiometry of these minerals. For example, in the Luobusa ophiolites, the composition of *in situ* alloys departs from that of isoferroplatinum, having a higher proportion of Fe + Ni + Cu (Bai *et al.* 2000). Pt–Fe alloys commonly show variable and locally high solubilities of Rh, Ir, Os, Pd, Ni and Cu (Cabri *et al.* 1977, 1996, Johan *et al.* 1990, Slansky *et al.* 1991, Bai *et al.* 2000, Tolstykh *et al.* 2000). High Rh contents have been measured in some instances: Pt–Fe alloys from *in situ* mineralization occurring at Thetford Mines (Corrivaux & Laflamme 1990), Tropoja (Ohnenstetter *et al.* 1999), New Caledonia (Augé *et al.* 1998), and in Luobusa (Bai *et al.* 2000), where Rh is replacing Pt in the chemical formula. RhFe, the Rh-dominant equivalent of tetraferroplatinum, locally occurs in Tropoja (Ohnenstetter *et al.* 1999). The local abundance of Rh-rich alloys within this deposit could be explained by the variable behavior of Rh in its dependence on $f(S_2)$, with the crystallization of Rh alloys preferred at very low $f(S_2)$, as documented in our experimental results. The presence of regularly spaced lamellae of PGE alloys and of Pt–Cu alloys in Pt–Fe nugget agrees with the former presence of high-temperature solid-solutions that exsolved Os-, Ir-, Ru-rich alloys or Cu-rich alloys during cooling (Johan *et al.* 1990, Slansky *et al.* 1991, Cabri *et al.* 1996, Augé *et al.* 1998). The level of Cu encountered in Pt–Fe alloys could be high, both in the ophiolites and in the Alaskan-type complexes, and prevents a clear discrimination between the two types of mineralization (Gornostayev *et al.* 1999). A similar conclusion is reached by considering the composition and parageneses of the associated PGM (Augé & Legendre 1992). However, according to Tolstykh *et al.* (2000), the presence of Ni-bearing minerals instead of Cu-bearing ones in ophiolites helps in determining the source of placers. Again, as for Rh, the high concentration of Cu and Pd in Pt–Fe alloys is well explained by the present experiments, as Cu and Pd may form alloys under very low fugacities of sulfur.

In addition, the experiments indicate that $f(S_2)$ should increase during the formation of a Pt deposit, as the residual liquid is directed toward the more Cu-rich composition. This should lead to the observation of zoned

assemblages, consisting of a centrally disposed Fe-rich alloy, surrounded by alloys rich in Pt. In fact, this is the opposite of the common observation in natural deposits, where tetraferroplatinum, commonly with tulameenite, are described as secondary minerals rimming isoferroplatinum (Corrivaux & Laflamme 1990, Cabri & Genkin 1991, Ohnenstetter *et al.* 1991). This zoned assemblage of minerals indicates that in addition to $f(S_2)$, other intensive parameters such as $f(O_2)$ may have controlled the successive deposition of alloys (Ertel *et al.* 1999, Amossé *et al.* 2000). From the experiments of Roeder & Jamieson (1992), we can suggest that the increase of Fe/(Fe + Pt) observed from the early-stage to the late-stage alloys could have resulted from more severely reducing conditions. The late-stage Cu-bearing alloys, such as tulameenite, generally associated with tetraferroplatinum, could be of primary origin, resulting from an increase of Cu activity in the residual sulfide melt, following the deposition of the early Pt–Fe alloys, or of secondary origin, arising by exsolution from a high-temperature Pt–Pd–Fe–Cu–Ni alloy solid-solution. We cannot exclude the possibility that the late-stage alloys could also form by reaction of magmatic alloys and sulfides with fluids during a late hydrothermal–magmatic stage or during serpentinization.

The existence of a Cu-rich melt hosting the light platinum-group elements Pt, Pd and Rh is indicated by the occurrence of spherical blebs of sulfide included in the Pt–Fe alloys. Johan *et al.* (1990) described an association of bornite with a Pd-rich sulfide, displaying a complex composition with a high content of Rh, Pt and Cu, and a metal:S value of 1.5. PGE-bearing phases and bornite were considered to have exsolved from a high-temperature complex Pt–Rh–Pd–Ir–Cu–Fe–Ni solid-solution. The anomalous composition of bornite, with excess copper, indicates an extensive solid-solution toward digenite, which may have formed at higher temperature from a Cu-rich melt. The existence of such a Pt-, Rh-, Pd- and Cu-rich melt locally trapped in the Pt–Fe alloys could indicate significant fractionation of Mss from the early-formed Fe-rich sulfide melt, leading to the residual Cu-rich liquid. However, Pt-, Rh-, Pd- and Cu-rich sulfide liquid trapped within Pt–Fe alloys may also have been derived by separation of sulfide melt into two liquids, one Fe-rich and the other Cu-rich. The first experimental evidence of such a process of "sulfide–sulfide" immiscibility was obtained during the study of phase relations in the system Fe–Ni–Cu–S at 1000°C (Peregoedova 1998, in press). In the S-undersaturated part of the system Fe–Ni–Cu–S (about 47–50 at.% S), a small area exists at 1000°C where two sulfide liquids coexist: an extremely Cu-rich but S-poor liquid (about 47 at.% S) and a relatively Fe- and S-rich liquid. Partition of the PGE between the two liquids occurs as follows: Pt and Pd are distributed preferentially into the Cu-rich liquid, whereas Rh accumulates in the Fe-rich liquid. The Cu- and precious-metals-enriched, S-poor residual liquid thus could have formed as a result of

sulfide–sulfide immiscibility from an already evolved Cu-rich sulfide melt. Multiphase parageneses comprising vysotskite, vasilite ($Pd_{16}S_7$), (Pt,Pd)$_3S_2$, (Pt,Pd,Fe, Cu)$_3$S, (Cu,Fe,Pd,Pt,Rh,Ru)$_9S_8$, bornite and chalcopyrite could represent the breakdown products of a residual Cu- and Pd-rich S-poor sulfide melt filling gas vesicles in nuggets of platinum (Tolstykh *et al.* 2000). On the other hand, inclusions of cooperite, cuprorhodsite and a Pd-rich sulfide in other nuggets of isoferroplatinum (Gornostayev *et al.* 1999) have bulk compositions suggestive of the existence of a late-stage sulfide melt richer in sulfur.

CONCLUSIONS

A complete solid-solution exists between heazlewoodite and intermediate solid-solutions at 760°C in the system Fe–Ni–Cu–S. The possibility of the direct crystallization of pentlandite from a Cu-bearing sulfide melt is considered unlikely, as primary pentlandite was not found to be stable in the high-temperature associations.

A distinctive feature of the physicochemical behavior of Pt is its early crystallization in the form of Fe–Pt alloys in association with Fe-rich BMS or in the form of sulfides in the Cu-rich compositions. The following limits of sulfur fugacity were established for various Pt-bearing phases stable in the BMS associations in the Me_9S_8 section at 760°C: log $f(S_2) \leq -10.5$ (in atm.) for γ(Fe,Ni,Pt) alloy; $-7.5 \leq$ log $f(S_2) \leq -5.5$ for PtFe; $-5.5 \leq$ log $f(S_2) \leq -4.1$ for Pt–Fe alloys richer in Pt; $-3.6 \leq$ log $f(S_2) \leq -1.7$ for PtS, and log $f(S_2) \geq -1.1$ for Cu(Pt,Ni)$_2S_4$. At 760°C, palladium is distributed among sulfide solid-solutions, with "quaternary" Hz–Iss its principal collector. The Pd content of Hz–Iss increases with enrichment of Hz–Iss in Cu and Ni, and attains 1.5 at.%. Rhodium is characterized by a dual behavior. Like palladium, it preferentially partitions into base-metal sulfides, especially into monosulfide solid-solution (up to 2.6 at.% Rh), but at conditions of very low or very high sulfur fugacity, it forms Rh minerals, as does platinum. Rh–Fe alloys are stable where log $f(S_2)$ is equal or less than -10.5, whereas the Rh sulfides [CuRh$_2S_4$ or (Rh,Ni)S$_2$] appear at conditions where log $f(S_2)$ is equal to or higher than -1.4.

The high-temperature Fe–Ni–Cu sulfide solid-solutions act as temporary collectors of the light PGE before the appearance of pentlandite during the formation of Cu–Ni–PGE ore. During cooling, the base-metal sulfide solid-solutions decompose, with palladium and rhodium partitioning into pentlandite or forming their own secondary minerals.

PGE deposits showing a predominance of Pt–Fe alloys, such as those in mantle rocks from ophiolites or nodules from kimberlites, are consistent with derivation from an S-poor sulfide melt. Zoned assemblages are compatible with the early crystallization of Pt–Fe alloys and a late-stage crystallization of Pd-rich high-temperature solid-solutions. This model could be applied to the

alloy type of PGE mineralization that occurs in some ophiolite cumulates and in the dunite core of Alaskan-type complexes, despite the scarcity of BMS. Even in these low-S deposits, a high fugacity of sulfur may be reached locally as a result of the appearance of a Cu-rich sulfide liquid derived by fractionation of an original Fe-rich sulfide melt or by immiscibility.

REFERENCES

AHMED, Z. & BEVAN, J.C. (1981): Awaruite, iridian awaruite, and a new Ru–Os–Ir–Ni–Fe alloy from the Sakhakot–Qila complex, Malakand Agency, Pakistan. *Mineral. Mag.* **44**, 225-230.

ALABUZHEV, B.A (1969): Differential thermal analysis plant. *In* Experimental Studies in Mineralogy 1968–1969 (A.A. Godovikov & V.S. Sobolev, eds.). IGG Siberian Branch, Russian Academy of Sciences, Novosibirsk, Russia (168-175). (in Russ.).

AMOSSÉ, J., DABLE, P. & ALLIBERT, M. (2000): Thermo-chemical behavior of Pt, Ir, Rh and Ru vs fO_2 and fS_2 in a basaltic melt. Implications for the differentiation and precipitation of these elements. *Mineral. Petrol.* **68**, 29-62.

AUGÉ, T., CABRI, L.J, LEGENDRE, O., MCMAHON, G. & COCHERIE, A. (1999): PGE distribution in base-metal alloys and sulfides of the New Caledonia ophiolite. *Can. Mineral.* **37**, 1147-1161.

_____ & LEGENDRE, O. (1992): Pt–Fe nuggets from alluvial deposits in eastern Madagascar. *Can. Mineral.* **30**, 983-1004.

_____, _____ & MAURIZOT, P. (1998): The distribution of Pt and Ru–Os–Ir minerals in the New Caledonia ophiolite. *In* International Platinum (N. Laverov & V.V. Distler, eds.). Theophrastus publications, St-Petersburg, Russia (141-154).

_____ & MAURIZOT, P. (1995): Stratiform and alluvial platinum mineralization in the New Caledonia ophiolite complex. *Can. Mineral.* **33**, 1023-1045.

BAI, WENJI, ROBINSON, P.T., FANG, QINGSONG, YANG, JINGSUI, YAN, BINGGANG, ZHANG, ZHONGMING, HU, XU-FENG, ZHOU, MEI-FU & MALPAS, J. (2000): The PGE and base-metal alloys in the podiform chromitites of the Luobusa ophiolites, southern Tibet. *Can. Mineral.* **38**, 585-598.

BALLHAUS, C. & SYLVESTER, P. (2000): Noble metal enrichment processes in the Merensky Reef, Bushveld Complex. *J. Petrol.* **41**, 545-561.

_____ & ULMER, P. (1995): Platinum-group elements in the Merensky reef. II. Experimental solubilities of platinum and palladium in $Fe_{1-x}S$ from 950 to 450°C under controlled fS_2 and fH_2. *Geochim. Cosmochim. Acta* **59**, 4881-4888.

BARKOV, A.Y., HALKOAHO, T.A.A., LAAJOKI, K.V.O., ALAPIETI, T.T. & PEURA, R.A. (1997): Ruthenian pyrite and nickeloan malanite from the Imandra layered complex, northwestern Russia. *Can. Mineral.* **35**, 887-897.

BARNES, S.-J. & MAIER, W.D. (2002): Platinum-group elements and microstructures of normal Merensky Reef from Impala Platinum Mines, Bushveld Complex. *J. Petrol.* **43**, 103-128.

_____, MAKOVICKY, E., MAKOVICKY, M., ROSE-HANSEN, J. & KARUP-MØLLER, S. (1997): Partition coefficients for Ni, Cu, Pd, Pt, Rh and Ir between monosulfide solid solution and sulfide liquid and the formation of compositionally zoned Ni–Cu sulfide bodies by fractional crystallization of sulfide liquid. *Can. J. Earth Sci.* **34**, 366-374.

_____, NALDRETT, A.J. & GORTON, M.P. (1985): The origin of the fractionation of platinum-group elements in terrestrial magmas. *Chem. Geol.* **53**, 303-323.

BARTON, P.B., JR. (1973): Solid-solution in the system Cu–Fe–S. 1. The Cu–S and CuFe–S join. *Econ. Geol.* **68**, 445-465.

BRENAN, J.M. & ANDREWS, D. (2001): High-temperature stability of laurite and Ru–Os–Ir alloy and their role in PGE fractionation in mafic magmas. *Can. Mineral.* **39**, 341-360.

CABRI, L.J. (1973): New data on phase relations in the Cu–Fe–S system. *Econ. Geol.* **68**, 443-454.

_____ & GENKIN, A.D. (1991): Re-examination of Pt alloys from lode and placer deposits, Urals. *Can. Mineral.* **29**, 419-425.

_____, HARRIS, D. & WEISER, T. (1996): Mineralogy and distribution of platinum mineral (PGM) placer deposits of the world. *Explor. Mining Geol.* **5**, 73-167.

_____, ROSENZWEIG, A.& PINCH, W.W. (1977): Platinum-group minerals from Onverwacht. I. Pt–Fe–Cu–Ni alloys. *Can. Mineral.* **15**, 380-384.

CORRIVAUX, L. & LAFLAMME, J.H.G. (1990): Minéralogie des éléments du groupe du platine dans les chromitites de l'ophiolite de Thetford mines, Québec. *Can. Mineral.* **28**, 579-595.

CRAIG, J.R. & KULLERUD, G. (1969): Phase relations in the Cu–Fe–Ni–S system and their application to magmatic ore-deposits. *Econ. Geol., Monogr.* **4**, 344-358.

CZAMANSKE, G. & MOORE, J.G. (1977): Composition and phase chemistry of sulfide globules in basalt from the Mid-Atlantic Ridge rift valley near 37°N lat. *Geol. Soc. Am., Bull.* **88**, 587-599.

DISTLER, V.V., GROKHOVSKAIA, T.L., EVSTIGNEYEVA, T.L., SLUZHENIKIN, S.F., FILIMONOVA, A.A., DYUZHIKOV, O.A. & LAPUTINA, I.P. (1988): Distribution, mineral composition and zoning of copper – nickel ores. *In* Petrology of the Sulphide Magmatic Ore-Formation (I.D. Ryabchikov, ed.). Izdatelstvo Nauka, Moscow, Russia (in Russ.; 41-105).

_____, KULAGOV, E.A., SLUZHENIKIN, S.F. & LAPUTINA, I.P. (1996): Quenched sulfide solid-solutions in the ores of Noril'sk deposit. *Geology of Ore Deposits* **38**, 41-53 (in Russ.).

_____, MALEVSKY, A.YU. & LAPUTINA, I.P. (1977): Distribution of the platinoids between the pyrrhotite and pentlandite in crystallization of the sulphide melt. *Geochem. Int.* **14**, 30-40.

DUTRIZAC, J.E. (1976): Reactions in cubanite and chalcopyrite. *Can. Mineral.* **14**, 172-181.

EBEL, D.S. & CAMPBELL, A.J. (1998): Rhodium and palladium partitioning between copper–nickel-pyrrhotite and sulfide liquid. *Geol. Soc. Am., Abstr. Program* **30A**, 318.

_____ & NALDRETT, A.J. (1996): Fractional crystallization of sulfide ore liquids at high temperatures. *Econ. Geol.* **91**, 607-621.

_____ & _____ (1997): Crystallization of sulfide liquids and the interpretation of ore composition. *Can. J. Earth Sci.* **34**, 352-365.

ERTEL, W., O'NEILL, H. ST.C., SYLVESTER, P.J. & DINGWELL, D.B. (1999): Solubilities of Pt and Rh in a haplobasaltic silicate melt at 1300°C. *Geochim. Cosmochim. Acta* **63**, 2439-2449.

EVSTIGNEEVA, T. & TARKIAN, M. (1996): Synthesis of platinum-group minerals under hydrothermal conditions. *Eur. J. Mineral.* **8**, 549-564.

FLEET, M.E., CHRYSSOULIS, S.L., STONE, W.E. & WEISENER, C.G. (1993): Partitioning of platinum-group elements and Au in the Fe–Ni–Cu–S system: experiments on the fractional crystallization of sulfide melt. *Contrib. Mineral. Petrol.* **115**, 36-44.

_____ & PAN, YUANMING (1994): Fractional crystallization of anhydrous sulfide liquid in the system Fe–Ni–Cu–S, with application to magmatic sulfide deposits. *Geochim. Cosmochim. Acta* **58**, 3369-3377.

_____ & STONE, W. (1991): Partitioning of platinum-group elements in the Fe–Ni–S system and their fractionation in nature. *Geochim. Cosmochim. Acta* **55**, 245-253.

_____, _____ & CROCKET, J.H. (1991): Partitioning of palladium, iridium, and platinum between sulfide liquid and basalt melt: effects of melt composition, concentration and oxygen fugacity. *Geochim. Cosmochim. Acta* **55**, 2545-2554.

FYODOROVA, Z.N. & SINYAKOVA, E.F. (1993): Experimental investigation of physicochemical conditions of pentlandite formation. *Russ. Geol. Geophys.* **34**, 79-87.

GARUTI, G., GAZZOTTI, M. & TORRES-RUIZ, J. (1995): Iridium, rhodium, and platinum sulfides in chromitites from the ultramafic massifs of Finero, Italy, and Ojen, Spain. *Can. Mineral.* **33**, 509-520.

GAUTHIER, M., CORRIVAUX, L., TROTTIER, L.J., CABRI, J., LAFLAMME, J.H.G. & BERGERON, M. (1990): Chromitites platinifères des complexes ophiolitiques de l'Estrie–Beauce, Appalaches du sud du Québec. *Mineral. Deposita* **25**, 169-178.

GORNOSTAYEV, S.S., CROCKET, J.H., MOCHALOV, A.G. & LAAJOKI, K.V.O. (1999): The platinum-group minerals of the Baimka placer deposits, Aluchin horst, Russian Far East. *Can. Mineral.* **37**, 1117-1129.

_____, OHNENSTETTER, M., NEZIRAJ, A., OHNENSTETTER, D., LAAJOKI, K.V.O., POPOVCHENKO, S.E. & KORNIENKO, P.K. (2001): New occurrences of anduoite (Ru,Os)As$_2$, from chromite deposits of Ukraine and Albania. *Can. Mineral.* **39**, 591-606.

GUILLON, J.H. & LAWRENCE, L.J. (1973): The opaque minerals of the ultramafic rocks of New Caledonia. *Mineral. Deposita* **8**, 115-126.

HAMLYN, P.R., KEAYS, R.R., CAMERON, W.E., CRAWFORD, A.J. & WALDRON, H.M. (1985): Precious metals in magnesian low-Ti lavas: implications for metallogenesis and sulfur saturation in primary magmas. *Geochim. Cosmochim. Acta* **49**, 1797-1811.

HILL, R.E.T. (1983): Experimental study of phase relations at 600°C in a portion of the Fe–Ni–Cu–S system and its application to natural sulphide assemblages. *In* Sulphide Deposits in Mafic and Ultramafic Rocks. (D.L. Buchanan & M.J. Jones, eds.). Institution of Mining and Metallurgy, London, U.K. (14-21).

HSIEH, K.C., CHANG, Y.A. & ZHONG, T. (1982): The Fe–Ni–S system above 700°C (iron – nickel – sulfur). *Bull. Alloy Phase Diagrams* **3**, 165-172.

HUTCHINSON, D., PRICHARD, H.M. & MACLEOD, C.J. (1999): Evidence for partial melting and melt impregnation of mantle peridotites leading to PGM deposition: a comparison of samples from the Lizard and Troodos ophiolites and the Tonga trench. *In* Mineral Deposits: Processes to Processing **1** (C.J. Stanley *et al.* eds.). Balkema, Rotterdam, The Netherlands (729-732).

JOHAN, Z., OHNENSTETTER, M., FISCHER, W. & AMOSSÉ, J. (1990): Platinum-group minerals from the Durance River alluvium, France. *Mineral. Petrol.* **42**, 287-306.

_____, SLANSKY, E. & OHNENSTETTER, M. (1991): Isoferroplatinum nuggets from Milverton (Fifield, N.S.W., Australia): a contribution to the origin of PGE mineralization in Alaskan-type complexes. *C.R. Acad. Sci. Paris* **312**, 55-60.

KARUP-MØLLER, S. & MAKOVICKY, E. (1995): The phase system Fe–Ni–S at 725°C. *Neues Jahrb. Mineral., Monatsh.*, 1-10.

_____ & _____ (1998): The phase system Fe–Ni–S at 900°C. *Neues Jahrb. Mineral., Monatsh.*, 373-384.

KINLOCH, E.D. (1982): Regional trends in the platinum-group mineralogy of the Critical Zone of the Bushveld Complex, South Africa. *Econ. Geol.* **77**, 1328-1347.

KOLONIN, G.R. (1998): Organizational principles and structure of mineral equilibria database in PGE-containing sulfide systems. *Russ. Geol. Geophys.* **39**, 1237-1244.

_____, PEREGOEDOVA, A.V., SINYAKOVA, E.F. & FEDOROVA, Z.N. (1993): On accordance between platinum mineral forms and ore-forming sulphide assemblages (experimental data). *Dokl. Russ. Akad. Nauk* **332**, 364-367 (in Russ.).

KULLERUD, G. (1963): Thermal stability of pentlandite. *Can. Mineral.* **7**, 353-366.

_____, YUND, R.A. & MOH, G.H. (1969): Phase relations in the Cu–Fe–S, Cu–Ni–S and Fe–Ni–S systems. *Econ. Geol., Monogr.* **4**, 323-343.

LI, CHUSI, BARNES, S.-J., MAKOVICKY, E., ROSE-HANSEN, J. & MAKOVICKY, M. (1996): Partitioning of nickel, copper, iridium, rhodium, platinum, and palladium between monosulfide solid-solution and sulfide liquid: effects of composition and temperature. *Geochim. Cosmochim. Acta* **60**, 1231-1238.

_____, NALDRETT, A.J., COATS, C.J.A. & JOHANNESSEN, P. (1992): Platinum, palladium, gold and copper-rich stringers at Strathcona mine, Sudbury: their enrichment by fractionation of a sulfide liquid. *Econ. Geol.* **87**, 1584-1598.

LINÉ, G. & HUBER, M. (1963): Etude radiocristallographique à haute température de la phase nonstoechiométrique Ni$_{3\pm x}$S$_2$. *C.R. Acad. Sci. Paris* **256**, 3118-3120.

LORAND, J.P., KEAYS, R.R. & BODINIER, J.L. (1993): Copper and noble metal enrichments across the lithosphere–asthenosphere boundary of mantle diapirs: evidence from the Lanzo lherzolite massif. *J. Petrol.* **34**, 1111-1140.

MAIER, W.D. & BARNES, S.-J. (1999): Platinum-group elements in silicate rocks of the Lower, Critical and Main zones at Union section, western Bushveld Complex. *J. Petrol.* **40**, 1647-1671.

MAKOVICKY, M., MAKOVICKY, E. & ROSE-HANSEN, J. (1986): Experimental studies on the solubility and distribution of platinum-group elements in base-metal sulphides in platinum deposits. *In* Metallogeny of Basic and Ultrabasic Rocks (M.J. Gallagher, R.A. Ixer, C.R. Neary & H.M. Prichard, eds.). The Institution of Mining and Metallurgy, London, U.K. (415-425).

MCLAREN, C.H. & DE VILLIERS, J.P.R. (1982): The platinum-group chemistry and mineralogy of the UG2 chromitite layer of the Bushveld Complex. *Econ. Geol.* **77**, 1348-1366.

MELCHER, F., GRUM, W., SIMON, G., THALHAMMER, T.V. & STUMPFL, E.F. (1997): Petrogenesis of the ophiolitic giant chromite deposits of Kempirsai, Kazakhstan: a study of solid and fluid inclusions in chromite. *J. Petrol.* **38**, 1419-1458.

MOSTERT, A.B., HOFMAYR, P.K. & POTGIETER, G.A. (1982): The platinum-group mineralogy of the Merensky Reef at the Impala Platinum Mines, Bophuthatswana. *Econ. Geol.* **77**, 1385-1394.

NALDRETT, A.J. (1967): Partial pressure of sulfur in the vapor coexisting with the Fe$_{1-x}$S–Ni$_{1-x}$S solid-solution at 600°C. *Carnegie Inst. Wash., Yearbook* **65**, 326-328.

_____ (1989): *Magmatic Sulfide Deposits*. Clarendon Press, New York, N.Y.

_____, CRAIG, J.R. & KULLERUD G. (1967): The central portion of the Fe–Ni–S system and its bearing on pentlandite exsolution in iron–nickel sulfide ores. *Econ. Geol.* **62**, 826-847.

_____, EBEL, D.S., ARIF, M., MORRISON, G. & MOORE, C.M. (1997): Fractional crystallization of sulphide melts as illustrated at Noril'sk and Sudbury. *Eur. J. Mineral.* **9**, 365-377.

_____ & KULLERUD, G. (1967): Limits of the Fe$_{1-x}$S – Ni$_{1-x}$S solid-solution between 600°C and 250°C. *Carnegie Inst. Wash., Yearbook* **65**, 320-326.

NIXON, G.T., CABRI, L.J. & LAFLAMME, J.H.G. (1990): Platinum-group-element mineralization in lode and placer deposits associated with the Tulameen Alaskan-type complex, British Columbia. *Can. Mineral.* **28**, 503-535.

OHNENSTETTER, M. (1992): Platinum-group element enrichment in the upper mantle peridotites of the Monte Maggiore ophiolitic massif (Corsica, France): mineralogical evidence for ore–fluid metasomatism. *Mineral. Petrol.* **46**, 85-107.

_____ (1996): Diversity of PGE deposits in basic–ultrabasic intrusives – single model of formation. *In* Petrology and Geochemistry of Magmatic Suites of Rocks in the Continental and Oceanic Crusts. A Volume Dedicated to Professor Jean Michot (D. Demaiffe, ed.). Université Libre de Bruxelles, Bruxelles, and Royal Museum for Central Africa, Tervuren, Belgium (337-354).

_____, JOHAN, Z., COCHERIE, A., FOUILLAC, A.M., GUERROT, C., OHNENSTETTER, D., CHAUSSIDON, M., ROUER, O., MAKOVICKY, E., MAKOVICKY, M., ROSE-HANSEN, J., KARUP-MØLLER, S., VAUGHAN, D., TURNER, G., PATTRICK, R.A.D., GIZE, A.P., LYON, I. & McDONALD, I. (1999): New exploration methods for platinum and rhodium deposits poor in base-metal sulphides – NEXTPRIM. *Trans. Inst. Mining Metall.* **108**, B119-B150.

_____, KARAJ, N., NEZIRAJ, A., JOHAN, Z. & ÇINA, A. (1991): Le potentiel platinifère des ophiolites: minéralisations en éléments du groupe du platine (EGP) dans les massifs de Tropoja et Bulqiza, Albanie. *C.R. Acad. Sci. Paris* **313**, *Sér.* **II**, 201-208.

PASTERIS, J.D. (1984): Further interpretation of the Cu–Fe–Ni sulfide mineralization in the Duluth complex, northeastern Minnesota. *Can. Mineral.* **22**, 39-53.

PEREGOEDOVA, A. (1998): The experimental study of the Pt–Pd-partitioning between monosulfide solid-solution and Cu–Ni-sulfide melt at 900–840°C. *8th Int. Platinum Symp.* (*Johannesburg*), 325-327 (abstr.).

_____ (in press): Distribution of platinum-group elements on the high temperature stage of sulfide ore-formation (experimental data). *In* Collected Articles of Young Scientists of Siberian Branch, Russian Academy of Sciences, Novosibirsk, Russia (in Russ.).

_____ & OHNENSTETTER, M. (1999): Experimental data on palladium- and rhodium-bearing pentlandite, with application to natural Cu–Ni–PGE sulphide ores. *X European Union of Geosciences, Strasbourg, France* (abstr.). *J. Conf. Abstr.* **4**, 484.

POUCHOU, J.-L. & PICHOIR, F. (1984): Un nouveau modèle de calcul pour la microanalyse quantitative par spectrométrie de rayons X. *Recherche Aérospatiale* **3**, 167-192.

_____ & _____ (1991): Quantitative analysis of homogeneous or stratified microvolumes applying the model "PAP". *In* Electron Probe Quantitation (K.F.J. Heinrich & D.E. Newbury, eds.). Plenum Press, New York, N.Y. (31-75).

ROEDER, P.L. & JAMIESON, H.E. (1992): Composition of chromite and co-existing Pt–Fe alloy at magmatic temperatures. *Aust. J. Earth Sci.* **39**, 419-426.

SHEWMAN, R.W. & CLARK, L.A. (1970): Pentlandite phase relations in the Fe–Ni–S system and notes on the monosulfide solid-solution. *Can. J. Earth. Sci.* **7**, 67-85.

SINYAKOVA, E.F., FEDOROVA, Z.N. & PAVLUCHENKO, V.S. (1996): Physicochemical conditions of formation of platinum phases in the system Fe–Ni–S. *Russ. Geol. Geophys.* **37**, 38-47.

_____, _____, SEREDKIN, YU.V. & DEMENSKYI, G.K. (1991): A study of subsolidus phase transformations of pentlandite on heating. *Proc. XII All-Union Conf. on Experimental Mineralogy,* The Institute of Experimental Mineralogy of Academy of Sciences of USSR, Chernogolovka, 20 (in Russ.).

_____, KOSYAKOV, V.A. & SHESTAKOV, V.A. (1999): Investigation of the surface of the liquidus of the Fe–Ni–S system at $X_s < 0.51$. *Metall. Mat. Trans.* **30B**, 715-722.

SLANSKY, E., JOHAN, Z., OHNENSTETTER, M., BARRON, L.M. & SUPPEL, D. (1991): Platinum mineralization in the Alaskan-type intrusive complexes near Fifield, N.S.W., Australia. 2. Platinum-group minerals in placer deposits at Fifield. *Mineral. Petrol.* **43**, 161-180.

STONE, W.E. & FLEET, M.E. (1990): Platinum–iron alloy (Pt₃Fe) in kimberlite from Fayette County, Pennsylvania. *Am. Mineral.* **75**, 881-885.

SUGAKI, A. & KITAKAZE, A. (1998): High form of pentlandite and its thermal stability. *Am. Mineral.* **83**, 133-140.

TISTL, M. (1994): Geochemistry of platinum-group elements of the zoned ultramafic Alto Condoto complex, northwest Colombia. *Econ. Geol.* **89**, 158-167.

TOLSTYKH, N.D., SIDOROV, E.G., LAAJOKI, K.V.O., KRIVENKO, A.P. & PODLIPSKY, M. (2000): The association of platinum-group minerals in placers of the Pustaya river, Kamchatka, Russia. *Can. Mineral.* **38**, 1251-1264.

TOULMIN, P., III & BARTON, P.B., JR. (1964): A thermodynamic study of pyrite and pyrrhotite. *Geochim. Cosmochim. Acta* **28**, 641-671.

TREDOUX, M., LINDSAY, N.M., DAVIES, G., & McDONALD, I. (1995): The fractionation of platinum-group elements in magmatic systems, with the suggestion of a novel causal mechanism. *S. Afr. J. Geol.* **98**, 157-167.

VERMAAK, C. F. & HENDRICKS, L.P. (1976): A review of the mineralogy of the Merensky Reef with specific reference to new data on the precious metal mineralogy. *Econ. Geol.* **71**, 1244-1269.

VON GRUENEWALDT, G., DICKS, D., DE WET, J. & HORSH, H. (1990): PGE mineralization in the western sector of the eastern Bushveld Complex. *Mineral. Petrol.* **42**, 71-95.

YANG, KAI. & SECCOMBE, P.K. (1993): Platinum-group minerals in the chromitites from the Great Serpentinite Belt, NSW, Australia. *Mineral. Petrol.* **47**, 263-286.

WEISER, T.W. & BACHMAN, H.G. (1999): Platinum-group minerals from the Aikora River area, Papua New Guinea. *Can. Mineral.* **37**, 1131-1145.